

University of Dundee

## The re-polarisation of M2 and M1 macrophages and its role on cancer outcomes

den Breems, Nicoline Y.; Eftimie, Raluca

*Published in:*  
Journal of Theoretical Biology

*DOI:*  
[10.1016/j.jtbi.2015.10.034](https://doi.org/10.1016/j.jtbi.2015.10.034)

*Publication date:*  
2016

*Licence:*  
CC BY-NC-ND

*Document Version*  
Peer reviewed version

[Link to publication in Discovery Research Portal](#)

*Citation for published version (APA):*  
den Breems, N. Y., & Eftimie, R. (2016). The re-polarisation of M2 and M1 macrophages and its role on cancer outcomes. *Journal of Theoretical Biology*, 390, 23-39. <https://doi.org/10.1016/j.jtbi.2015.10.034>

### General rights

Copyright and moral rights for the publications made accessible in Discovery Research Portal are retained by the authors and/or other copyright owners and it is a condition of accessing publications that users recognise and abide by the legal requirements associated with these rights.

- Users may download and print one copy of any publication from Discovery Research Portal for the purpose of private study or research.
- You may not further distribute the material or use it for any profit-making activity or commercial gain.
- You may freely distribute the URL identifying the publication in the public portal.

### Take down policy

If you believe that this document breaches copyright please contact us providing details, and we will remove access to the work immediately and investigate your claim.



**University of Dundee**

## **The re-polarisation of M2 and M1 macrophages and its role on cancer outcomes**

den Breems, Nicoline; Eftimie, Raluca

*Published in:*  
Journal of Theoretical Biology

*DOI:*  
[10.1016/j.jtbi.2015.10.034](https://doi.org/10.1016/j.jtbi.2015.10.034)

*Publication date:*  
2016

*Document Version*  
Early version, also known as pre-print

[Link to publication in Discovery Research Portal](#)

*Citation for published version (APA):*  
den Breems, N., & Eftimie, R. (2016). The re-polarisation of M2 and M1 macrophages and its role on cancer outcomes. *Journal of Theoretical Biology*, 390, 23-39. [10.1016/j.jtbi.2015.10.034](https://doi.org/10.1016/j.jtbi.2015.10.034)

© 2016. This manuscript version is made available under the CC-BY-NC-ND 4.0 license <http://creativecommons.org/licenses/by-nc-nd/4.0/>

### **General rights**

Copyright and moral rights for the publications made accessible in Discovery Research Portal are retained by the authors and/or other copyright owners and it is a condition of accessing publications that users recognise and abide by the legal requirements associated with these rights.

- Users may download and print one copy of any publication from Discovery Research Portal for the purpose of private study or research.
- You may not further distribute the material or use it for any profit-making activity or commercial gain.
- You may freely distribute the URL identifying the publication in the public portal.

### **Take down policy**

If you believe that this document breaches copyright please contact us providing details, and we will remove access to the work immediately and investigate your claim.

# The re-polarisation of M2 and M1 macrophages and its role on cancer outcomes

Nicoline Y. den Breems<sup>a,b,c</sup>, Raluca Eftimie<sup>b,\*</sup>

<sup>a</sup>*Centre for Advanced Computational Solutions (C-fACS), Lincoln University, Lincoln, 7476, New Zealand*

<sup>b</sup>*Division of Mathematics, University of Dundee, Dundee, United Kingdom, DD1 4HN*

<sup>c</sup>*Division of Cancer Research, University of Dundee, Dundee, United Kingdom, DD1 9SY*

---

## Abstract

The anti-tumour and pro-tumour roles of Th1/Th2 immune cells and M1/M2 macrophages have been documented by numerous experimental studies. However, it is still unknown how these immune cells interact with each other to control tumour dynamics. Here, we use a mathematical model for the interactions between mouse melanoma cells, Th2/Th1 cells and M2/M1 macrophages, to investigate the unknown role of the re-polarisation between M1 and M2 macrophages on tumour growth. The results show that tumour growth is associated with a type-II immune response described by large numbers of Th2 and M2 cells. Moreover, we show that: (i) the ratio  $k$  of the transition rates  $k_{12}$  (for the re-polarisation M1→M2) and  $k_{21}$  (for the re-polarisation M2→M1) is important in reducing tumour population, and (ii) the particular values of these transition rates control the delay in tumour growth and the final tumour size. We also perform a sensitivity analysis to investigate the effect of various model parameters on changes in the tumour cell population, and confirm that the ratio  $k$  alone and the ratio of M2 and M1 macrophage populations at earlier times (e.g., day 7), cannot always predict the final tumour size.

*Keywords:* cancer modelling, M1 and M2 macrophages, Th1 and Th2 immune cells

*2010 MSC:* 92C50

---

\*Corresponding author.

*Email addresses:* nicoline.vanloenen@lincolnuni.ac.nz (Nicoline Y. den

## 1. Introduction

The anti-tumour role of the immune system has been documented for more than a century (McCarthy, 2006). Despite recent success with some types of immunotherapies (e.g., involving antibodies or cancer vaccines), many anti-tumour therapies are still not leading to the expected outcomes (Rosenberg et al., 2004). One reason is that there are still numerous questions regarding the biological mechanisms behind the interactions between the immune cells and tumour cells. The complexity of these interactions is acknowledged by the immunoediting hypothesis, which emphasises the dual role of the immune response: tumour-promoting and tumour-suppressing (Schreiber et al., 2011; Dunn et al., 2004). One of the mechanisms thought to be involved in the persistence and growth of tumours is the transition from a Th1- to a Th2-dominated environment, which appears to happen when the cancer microenvironment is dominated by cytokines such as IL-4 (synthesised by CD4<sup>+</sup>T cells) and growth factors like CSF1 and GM-CSF (Noy and Pollard, 2014). However, other studies have shown that both Th1- and Th2-dominated environments can successfully eliminate tumours independent of CD8<sup>+</sup>T cells (Nishimura et al., 1999; Hung et al., 1998; Perez-Diez et al., 2007), and in some cases the Th2-dominated environments are better at eliminating tumours compared to the Th1-dominated environments (Mattes et al., 2003). Overall, the mechanisms controlling the ratio of Th1/Th2 cells, and its role on tumour elimination are still not completely understood.

A second ratio that seems to have predictive outcome on tumour growth and patient prognosis involves the M1 and M2 macrophages (Ohri et al., 2009; Heusinkveld and van der Burg, 2011; Chen et al., 2011; Zhang et al., 2014). These macrophages were named after the Th1-Th2 cell nomenclature, despite the fact that there is actually a full spectrum of phenotypes between these two types of macrophage polarisation (Mantovani et al., 2004).

While many studies focused on the total numbers of tumour-infiltrating macrophages and their role on tumour growth and patient prognosis (Mattes et al., 2003; Zeni et al., 2007; Hammes et al., 2007; Bingle et al., 2002; Clear et al., 2010; Steidl et al., 2010), some of the results in these studies were contradictory (Heusinkveld and van der Burg, 2011). For example, several studies have shown that increased macrophage numbers correlate with poor patient prognosis (Bingle et al., 2002; Clear et al., 2010; Leek et al., 1996;

Steidl et al., 2010; Zeni et al., 2007; Hammes et al., 2007; Zijlmans et al., 2006). Other studies have shown that increased macrophage numbers correlate with better patient survival (Welsh et al., 2005). Note that many of these contradictory results were for the same type of cancer: e.g., non-small cell lung cancer in Zeni et al. (2007); Welsh et al. (2005). A possible explanation for these results is the type of macrophages that infiltrate the tumours: M1 versus M2 cells (Heusinkveld and van der Burg, 2011). However, detailed investigation of the phenotype of these tumour-infiltrating macrophages sometimes generated even more contradictory results. For example, Ohri et al. (2009) revealed that improved survival in patients with non-small cell lung cancer was associated with a higher density of M1 macrophages compared to M2 macrophages inside tumour islets (see Figure 2(a) in Ohri et al. (2009)). Moreover, the overall number of M1 and M2 macrophages was increased in patients with long survival times compared to patients with short survival times. In a different study, Ma et al. (2010) also showed an increase in the number of M1 macrophages inside islets of non-small lung cancers, for patients with improved survival. However, in contrast to the results in (Ohri et al., 2009), Ma et al. (2010) observed a slight decrease in the number of M2 macrophages in patients with long survival times compared to patients with short survival times (see Table 2 in Ma et al. (2010)). Moreover, in Ma et al. (2010), improved survival was associated with similar M1 and M2 densities in tumour islets. One last difference between the studies in (Ohri et al., 2009) and (Ma et al., 2010), which was not emphasised by the authors themselves but can be deduced by comparing the data for macrophage densities inside tumour islets, is the ratio of M2/M1 in long-term survival patients (with  $M2/M1 \approx 1$  in Ma et al. (2010) and  $M2/M1 < 1$  in Ohri et al. (2009)) and short-term survival patients (with  $M2/M1 > 1$  in Ma et al. (2010) and  $M2/M1 \approx 1$  in Ohri et al. (2009)). Note that none of these studies did associate the number of macrophages with tumour size, but only with the percentage of patient survival.

To propose hypotheses regarding the biological mechanisms behind the observed discrepancies in experimental and clinical data, we need to have a better understanding of the interactions between the M1 and M2 macrophages and other cells in the microenvironment, such as the Th1 and Th2 cells with which the macrophages interact via type-I (e.g., IFN- $\gamma$ , IL-12) and type-II (e.g., IL-4, IL-10) cytokines (Biswas and Mantovani, 2010).

While there are mathematical models that focus on the Th2/Th1 balance (Kogan et al., 2013; Kim et al., 2013; Gross et al., 2011; Eftimie et al.,

2010) and models that focus on the M2/M1 balance (Wang et al., 2012; Louzoun et al., 2014) in various immunological contexts, including cancer immunotherapies, there are no mathematical models that combine these two aspects.

The goal of this study is to investigate whether the variation in the M2/M1 ratio and the re-polarisation of macrophages accounts for the difference in tumour growth or tumour decay. To this end, we derive a new non-spatial mathematical model that describes the interactions between the tumour cells (which can be recognised or not by the immune cells) and two types of immune cells, namely macrophages (M1 and M2) and T helper (Th1 and Th2) cells. For the macrophages dynamics, we explicitly model the plasticity of these cells that can re-polarise into a M1 or M2 phenotype depending on the cytokine environment (i.e., type I cytokines such as IFN- $\gamma$  can lead to M1 macrophages, while type-II cytokines such as IL-10 can lead to M2 macrophages). While this model cannot address any questions regarding the spatial aspects of tumour-immune interactions, it offers a much simpler framework within which we can investigate these interactions. We then use this mathematical model to investigate the effect of the ratio M2/M1 on tumour growth for early and advanced tumours. We first investigate all possible steady states, and study the role of the ratio  $k = k_{12}/k_{21}$  of the re-polarisation rates between the M1 and M2 macrophages on these states and their stability. Next we investigate numerically the role of model parameters on the long-term dynamics of the tumour growth. Since the numerical results depend on various parameters, we also conduct a sensitivity analysis to decide which parameters are most likely to influence the tumour growth. Our analysis reveals that a ratio  $M2/M1 > 1$  can explain the growth in tumour size. However, for  $M2/M1 < 1$ , the variation in tumour growth cannot be explained by this ratio alone (see the discussion in Section 5.4).

We emphasise from the beginning that the results of this study depend on the mice experimental data we used to parametrise the model. In particular, we use mice melanoma data from (Chen et al., 2011) since it shows multiple time points and thus allows for better model parametrisation (as opposed to the data in Ohri et al. (2009); Ma et al. (2010) for small-cell lung cancers, that shows only one time point). While it will be interesting to investigate how the results change if we use human data, such an investigation is beyond the scope of current study.

The article is structured as follows. In Section 2 we describe in detail the new mathematical model for tumour-immune interactions. In Section 3 we

investigate the steady states of this model, and their stability. In Section 4 we study the dynamics of the model using numerical simulations. In Section 5 we perform a sensitivity analysis for the parameters and initial conditions of the model. We conclude in Section 6 with a summary and discussion of the results.

## 2. Model Description

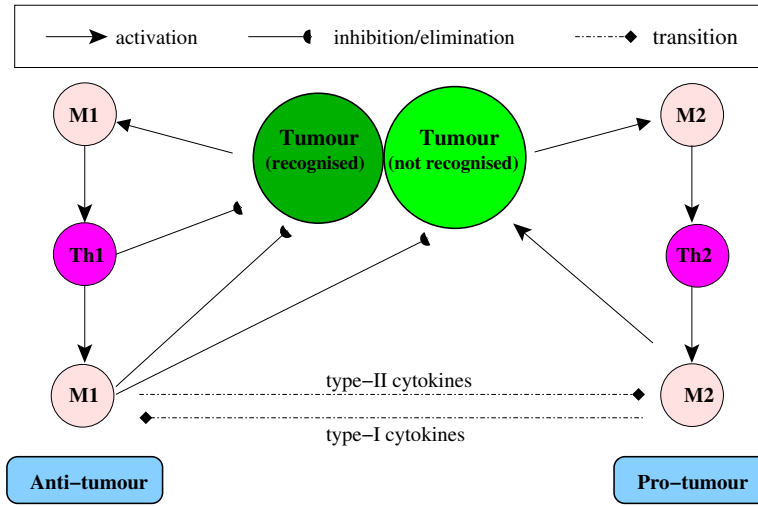


Figure 1: Schematic description of possible tumour-immune interactions, as suggested by various experimental results (Mattes et al., 2003; Mantovani et al., 2008; Baba et al., 2008; Biswas and Mantovani, 2010).

Throughout this article, we model and investigate the interactions of tumour cells ( $x_T$ ) with macrophages ( $x_M$ ) and Th cells ( $x_{Th}$ ). For the immune response, we model separately the dynamics of Th1 ( $x_{Th1}$ ) and Th2 ( $x_{Th2}$ ) cells, as well as the dynamics of M1 ( $x_{M1}$ ) and M2 ( $x_{M2}$ ) macrophages. For the tumour cells, we model the dynamics of immunogenic tumour cells ( $x_{Ts}$ ) that can be recognised (i.e., “seen”) by the immune cells, and non-immunogenic tumour cells ( $x_{Tn}$ ) that escape the surveillance by the immune system. To keep our mathematical model relatively simple, we will not model explicitly the type-I and type-II cytokines that mediate the interactions between M1 and Th1 cells, and between M2 and Th2 cells. These cytokine-mediated interactions will be modelled implicitly, by assuming that

the cytokines are produced by the macrophages and the Th cells. Thus, the time-evolution of all these cell densities is given by:

$$\frac{dx_{Tn}}{dt} = rx_{Tn} \left( 1 - \frac{x_{Tn} + x_{Ts}}{\beta_T} \right) + k_{sn}x_{Ts} - \delta_{mn}x_{M1}x_{Tn} + r_{mn}x_{Tn}x_{M2}, \quad (1a)$$

$$\frac{dx_{Ts}}{dt} = rx_{Ts} \left( 1 - \frac{x_{Tn} + x_{Ts}}{\beta_T} \right) - k_{sn}x_{Ts} - \delta_{ms}x_{M1}x_{Ts} - \delta_{ts}x_{Ts}x_{Th1}, \quad (1b)$$

$$\begin{aligned} \frac{dx_{M1}}{dt} = & (a_sx_{Ts} + a_{m1}x_{Th1})x_{M1} \left( 1 - \frac{x_{M1} + x_{M2}}{\beta_M} \right) - \delta_{m1}x_{M1} \\ & - k_{12}x_{M1}x_{M2} + k_{21}x_{M1}x_{M2}, \end{aligned} \quad (1c)$$

$$\begin{aligned} \frac{dx_{M2}}{dt} = & (a_nx_{Tn} + a_{m2}x_{Th2})x_{M2} \left( 1 - \frac{x_{M1} + x_{M2}}{\beta_M} \right) - \delta_{m2}x_{M2} \\ & + k_{12}x_{M1}x_{M2} - k_{21}x_{M1}x_{M2}, \end{aligned} \quad (1d)$$

$$\frac{dx_{Th1}}{dt} = a_{h1}x_{M1} + r_{h1}x_{M1}x_{Th1} \left( 1 - \frac{x_{Th1} + x_{Th2}}{\beta_{Th}} \right) - \delta_{h1}x_{Th1}, \quad (1e)$$

$$\frac{dx_{Th2}}{dt} = a_{h2}x_{M2} + r_{h2}x_{M2}x_{Th2} \left( 1 - \frac{x_{Th1} + x_{Th2}}{\beta_{Th}} \right) - \delta_{h2}x_{Th2}. \quad (1f)$$

These equations incorporate the following biological assumptions:

- Both tumour cell populations proliferate logistically at a rate  $r$ , to account for the slow-down in tumour growth due to lack of nutrients, as observed experimentally (Diefenbach et al., 2001; Laird, 1964). The  $x_{Ts}$  cells can mutate at a rate  $k_{sn}$  and become  $x_{Tn}$  cells. Also, the  $x_{Ts}$  cells can be eliminated at a rate  $\delta_{ts}$  by the adaptive immune response represented by the Th1 cells (Hung et al., 1998). Moreover, experimental studies have shown that the nonspecific macrophage reaction following the inoculation of tumour cells leads to the production of nitric oxide (cytotoxic for tumours; Xu et al. (2002)) in both immunogenic and non-immunogenic tumours (Kisseleva et al., 2001). Thus, we make the assumption that the M1 macrophages could eliminate the  $x_{Tn}$  cells at a rate  $\delta_{mn}$  and  $x_{Ts}$  cells at a rate  $\delta_{ms}$ , where we choose  $\delta_{mn} = \delta_{ms}$ ; see Table A.2. Moreover, we assume that the  $x_{Tn}$  cells can proliferate in the presence of M2 cells (Mills, 2012) at a rate  $r_{mn}$ . Even if the extracellular signals released by M2 cells could contribute also to the growth of  $x_{Ts}$  cells, the large mutation rate of mouse melanoma (Cillo et al., 1987) will lead to a fast transition from  $x_{Ts}$  to  $x_{Tn}$  cells. Thus,



for this study, we decided to ignore the potential contribution of  $x_{M2}$  macrophages to the growth of  $x_{Ts}$  cancer cells. Finally, we assume that the tumour cells die at rate much lower compared to the immune cells, and thus we ignore the natural death rate of  $x_{Tn}$  and  $x_{Ts}$  cells.

- The M1 macrophages proliferate at rate  $a_s$  in the presence of  $x_{Ts}$  tumour-specific antigens, and at rate  $a_{m1}$  in the presence of type I cytokines (which can be produced by Th1 cells, once these cells become activated) (Mantovani et al., 2004). Moreover the M1 macrophages have a half-life of  $1/\delta_{m1}$ . In addition, the cross-talk between the M1 and M2 macrophage-polarising signalling pathways can lead to a repolarisation, at rate  $k_{12}$ , of M1 cells into M2 cells (Sica and Bronte, 2007).
- The M2 macrophages proliferate at rate  $a_n$  in the presence of cytokines and growth factors produced by  $x_{Tn}$  cells, and at rate  $a_{m2}$  in the presence of type II cytokines (e.g., IL-4, which can be produced by Th2 cells, once these cells become activated) (Mantovani et al., 2004; Gordon and Martinez, 2010). The half-life of M2 macrophages is  $1/\delta_{m2}$ . For simplicity, throughout this study we will assume that  $\delta_{m2} = \delta_{m1}$ . Finally, the cross-talk between the M1 and M2 cells can lead to a repolarisation, at rate  $k_{21}$ , of M2 macrophages into M1 macrophages (Sica and Bronte, 2007).
- The Th1 cells are activated, at rate  $a_{h1}$ , by type-I cytokines (e.g., IFN- $\gamma$ ) that can be produced by the M1 macrophages (Romagnani, 1999; Sica and Mantovani, 2012). Also, they proliferate at rate  $r_{h1}$  in the presence of type-I cytokines produced by M1 cells, and have a half-life of  $1/\delta_{h1}$ .
- The Th2 cells are activated, at rate  $a_{h2}$ , by type-II cytokines that can be produced by the M2 macrophages (Romagnani, 1999; Sica and Mantovani, 2012). These Th cells proliferate at rate  $r_{h2}$  in the presence of type-II cytokines produced by the M2 cells, and have a half-life of  $1/\delta_{h2}$ .

Note that the terms that appear in model (1) are one of the multiple possible ways of describing the dynamics of tumour and immune cells. There are various models in the mathematical literature, where the growth and interaction rates of cells are assumed linear (not depending on direct or indirect

interactions with other cells); see, for example, [Louzoun et al. \(2014\)](#). Nevertheless, the goal of our study is not to investigate all these possible modelling approaches; rather is to choose one way of describing the interactions, and use it to investigate the anti-tumour type-I and type-II immune responses.

### 3. Steady states and their stability

To investigate the dynamics of system (1), we first focus on its long-term behaviour as described by the number and stability of the steady states. By calculating these states, we aim to emphasise the complex dynamics of equations (1), and the difficulty of fully understanding this dynamics.

#### 3.1. Tumour-free steady states

We first study the case when  $x_{Tn} = x_{Ts} = 0$ . For the baseline parameter values used here and listed in Table A.2, these tumour-free states are generally unstable (see the discussion in [AppendixC](#)). We therefore expect the dynamics of system (1) to move away from these states - as it will be confirmed in Sections 4,5 by the numerical simulations.

- Tumour-Free Immune-Free (TFIF) state:

$$(x_{Tn}^*, x_{Ts}^*, x_{M1}^*, x_{M2}^*, x_{Th1}^*, x_{Th2}^*) = (0, 0, 0, 0, 0, 0).$$

- Tumour-Free Type-I Immune response Present (TF1IP) state:

$$(x_{Tn}^*, x_{Ts}^*, x_{M1}^*, x_{M2}^*, x_{Th1}^*, x_{Th2}^*) = (0, 0, x_{M1}^*, 0, x_{Th1}^*, 0),$$

with  $x_{M1}^*$  and  $x_{Th1}^*$  given implicitly by the following equations:

$$x_{M1}^* = \frac{\delta_{h1} x_{Th1}^*}{a_{h1} + r_{h1} x_{Th1}^* (1 - \frac{x_{Th1}^*}{\beta_{Th}})} \quad \text{and} \quad x_{Th1}^* = \frac{\delta_{m1}}{a_{m1} (1 - \frac{x_{M1}^*}{\beta_M})}. \quad (2)$$

For the parameter values used throughout this article and given in Table A.2, there is a unique TF1IP steady state (see [AppendixB](#)).

- Tumour-Free Type-II Immune response Present (TF2IP) state:

$$(x_{Tn}^*, x_{Ts}^*, x_{M1}^*, x_{M2}^*, x_{Th1}^*, x_{Th2}^*) = (0, 0, 0, x_{M2}^*, 0, x_{Th2}^*),$$

with

$$x_{M2}^* = \frac{\delta_{h2} x_{Th2}^*}{a_{h2} + r_{h2} x_{Th2}^* (1 - \frac{x_{Th2}^*}{\beta_{Th}})} \quad \text{and} \quad x_{Th2}^* = \frac{\delta_{m2}}{a_{m2} (1 - \frac{x_{M2}^*}{\beta_M})}. \quad (3)$$

This state is also unique (see [AppendixB](#)).

- Tumour-Free Type-I and Type-II Immune-Present (TFIP) states:

$$(x_{Tn}, x_{Ts}, x_{M1}, x_{M2}, x_{Th1}, x_{Th2}) = (0, 0, x_{M1}^*, x_{M2}^*, x_{Th1}^*, x_{Th2}^*),$$

with  $x_{M1}^*, x_{M2}^*, x_{Th1}^*, x_{Th2}^*$  given implicitly by the following relations:

$$x_{M1}^* = \frac{\delta_{h1} x_{Th1}^*}{a_{h1} + r_{h1} x_{Th1}^* (1 - \frac{x_{Th1}^* + x_{Th2}^*}{\beta_{Th}})}, x_{M2}^* = \frac{\delta_{h2} x_{Th2}^*}{a_{h2} + r_{h2} x_{Th2}^* (1 - \frac{x_{Th1}^* + x_{Th2}^*}{\beta_{Th}})}, \quad (4a)$$

$$x_{Th1}^* = \frac{\delta_{m1} + k_{12} x_{M2}^* - k_{21} x_{M1}^*}{a_{m1} (1 - \frac{x_{M1}^* + x_{M2}^*}{\beta_M})}, x_{Th2}^* = \frac{\delta_{m2} - k_{12} x_{M1}^* + k_{21} x_{M1}^*}{a_{m2} (1 - \frac{x_{M1}^* + x_{M2}^*}{\beta_M})}. \quad (4b)$$

In contrast to the TF1IP and TF2IP states that are unique, there is an infinite number of TFIP states - see Figure B.13(A) in AppendixB. This emphasises the complexity of system (1), and the difficulty to predict its dynamics.

### 3.2. Tumour-present steady states

Next, we discuss the states where  $x_{Tn} > 0$ . Note that if  $x_{Tn} = 0$ , then we have also  $x_{Ts} = 0$ . The stability of the steady states with  $x_{Ts} = 0$  is discussed in AppendixC. The case  $x_{Ts} \neq 0$  is more complicated and it is very difficult to investigate analytically.

- Tumour-only (TO) states:

$$(x_{Tn}^*, x_{Ts}^*, x_{M1}^*, x_{M2}^*, x_{Th1}^*, x_{Th2}^*) = (x_{Tn}^*, \beta_T - x_{Tn}^*, 0, 0, 0, 0),$$

where for  $x_{Ts}^* = 0$  we have  $x_{Tn}^* = \beta_T$ . For the baseline parameter values used in this article and described in Table A.2, these states are always unstable (see AppendixC). Thus the dynamics of system (1) will never approach the TO states.

- Tumour-Present Type-I Immune Response Present (TP1IP) states:

$$(x_{Tn}^*, x_{Ts}^*, x_{M1}^*, x_{M2}^*, x_{Th1}^*, x_{Th2}^*) = (x_{Tn}^*, 0, x_{M1}^*, 0, x_{Th1}^*, 0),$$

with

$$x_{Tn}^* = \frac{\beta_T}{r}(r - \delta_{mn}x_{M1}^*), \quad (5a)$$

$$x_{M1}^* = \frac{\delta_{h1}x_{Th1}^*}{a_{h1} + r_{h1}x_{Th1}^*(1 - \frac{x_{Th1}^*}{\beta_{Th}})}, \quad x_{Th1}^* = \frac{\delta_{m1}}{a_{m1}(1 - \frac{x_{M1}^*}{\beta_M})}. \quad (5b)$$

For the baseline parameter values used in this article, the TP1IP state is unique (see [AppendixB](#)). Moreover this state is unstable and the dynamics of system (1) will not evolve towards it (see [AppendixC](#)).

- Tumour-Present Type-II Immune Response Present (TP2IP) states:

$$(x_{Tn}^*, x_{Ts}^*, x_{M1}^*, x_{M2}^*, x_{Th1}^*, x_{Th2}^*) = (x_{Tn}^*, 0, 0, x_{M2}^*, 0, x_{Th2}^*),$$

with

$$x_{Tn}^* = \frac{\beta_T}{r}(r + r_{mn}x_{M2}^*), \quad (6a)$$

$$x_{M2}^* = \frac{\delta_{h2}x_{Th2}^*}{a_{h2} + r_{h2}x_{Th2}^*(1 - \frac{x_{Th2}^*}{\beta_{Th}})}, \quad x_{Th2}^* = \frac{\delta_{m2} - a_n x_{Tn}^*(1 - \frac{x_{M2}^*}{\beta_M})}{a_{m2}(1 - \frac{x_{M2}^*}{\beta_M})}. \quad (6b)$$

Also this state is unique and stable for the parameter values used in this article - as confirmed by the numerical simulations in [Figure 3](#).

- Tumour-Present Immune-Present (TPIP) states:

$$(x_{Tn}^*, x_{Ts}^*, x_{M1}^*, x_{M2}^*, x_{Th1}^*, x_{Th2}^*),$$

with  $x_{Ts}^* = 0$  or  $x_{Ts}^* > 0$ . As we will see throughout the next sections, for the parameter values used in this article, system (1) usually approaches a TPIP state with  $x_{Ts}^* = 0$ . We emphasise here that the TPIP states are not unique, as shown in [Figure B.13\(B\)](#). The existence of these multiple states makes it difficult to investigate analytically their stability. However, the numerical results in the next sections suggest that the stability of these states depends also on the ratio  $k = k_{12}/k_{21}$ .

## 4. Numerical results

Next, we study the dynamics of model (1) through numerical simulations using ODE23tb in MATLAB©2013b. Since we want to understand

241 the mechanisms behind the change in the M2/M1 ratio, we fit several model  
 242 parameters to experimental data from [Chen et al. \(2011\)](#), who focused on  
 243 melanoma studies in mice (see Figure 2). In particular we study numer-  
 244 ically the effect of injecting on day zero  $10^6 x_{Ts}$  tumour cells and  $10^3 x_{Tn}$   
 245 tumour cells. We also assume that  $x_{Th1}(0) = 0$ ,  $x_{Th2}(0) = 0$  (i.e., no activ-  
 246 ated immune cells at the time of the injection). However, a small number of  
 247 tissue macrophages can be present at the injection site:  $x_{M1}(0) = 100$  and  
 248  $x_{M2}(0) = 100$ . For an extended overview of the model variables and paramet-  
 249 ers, and a description of the experimental setup see [Appendix A](#) and Tables  
 250 [A.1](#) & [A.2](#). Figure 2A compares the dynamics of  $x_{Tn} + x_{Ts}$  cells with tumour  
 251 data from [Chen et al. \(2011\)](#), to identify the parameter values for tumour  
 252 growth. Figure 2B compares the numbers of  $x_{M1}$  and  $x_{M2}$  cells on days 7  
 253 and 14 with macrophages data from [Chen et al. \(2011\)](#) (to identify parameter  
 254 values that govern the macrophage dynamics; see also [Appendix A](#)).

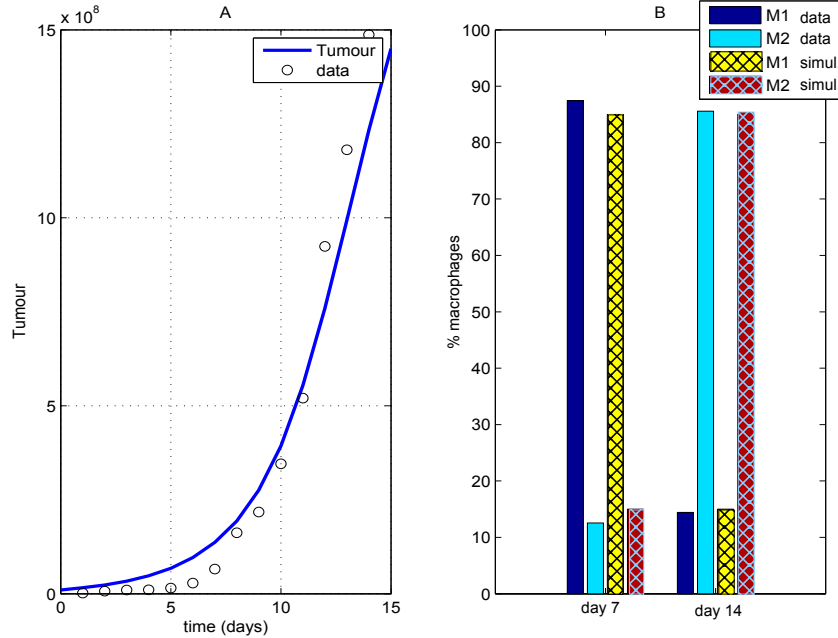


Figure 2: (A) Numerical simulation of tumour growth in model (1) compared to data from [Chen et al. \(2011\)](#) for the melanoma growth in mice; (B) The change in percentage of M1 and M2 macrophages at day 7 and day 14 for our numerical simulations and the experimental values shown in [Chen et al. \(2011\)](#).

Figure 3 shows the dynamics of tumour and immune cells, for the parameter values identified through comparison with the data (see Tables A.1 and A.2). We first notice that the  $x_{Tn}$  cells grow to the carrying capacity while the  $x_{Ts}$  cells are eliminated (Fig. 3A). Moreover, as seen in the experimental results (Fig. 2B), there is a shift in the macrophage profile: from a  $x_{M1}$  profile for  $t < 10$  days to a  $x_{M2}$  profile for  $t > 10$  days (Fig. 3B). This shift is accompanied by a shift in the Th profile: from a Th1-dominated dynamics during the first  $\approx 15$  days (Fig. 3C) to a Th2-dominated dynamics at a later time (Fig. 3D). Finally, we emphasise that for these particular parameter values, the long-term dynamics of model (1) approaches the TP2IP steady state; see equations (6).

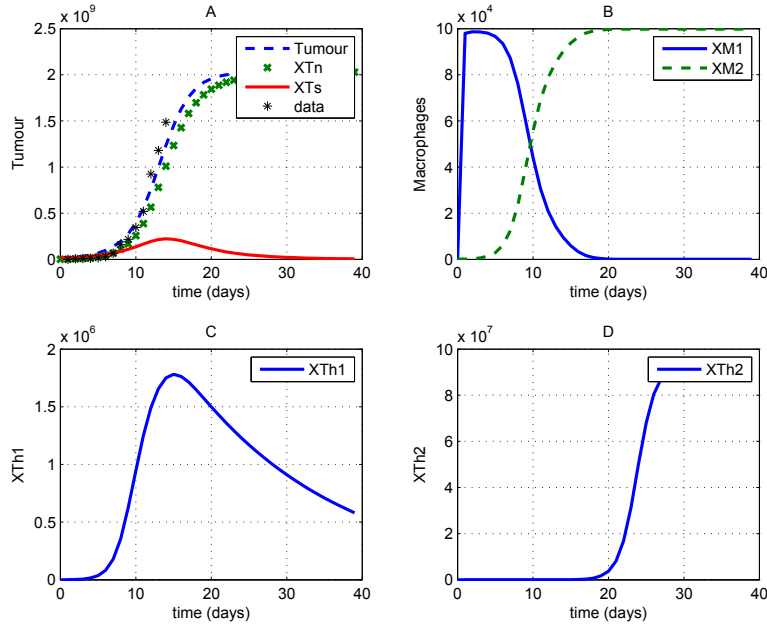


Figure 3: Dynamics of tumour and immune cells, for the initial conditions and parameter values described in Tables A.1 and A.2. (A) Total number of tumour cells (dashed curve),  $x_{Tn}$  cells (crosses) and  $x_{Ts}$  cells (continuous curve). For comparison purposes, we also show tumour data from Chen et al. (2011); (B)  $x_{M1}$  and  $x_{M2}$  macrophages; (C)  $x_{Th1}$  cells; (D)  $x_{Th2}$  cells.

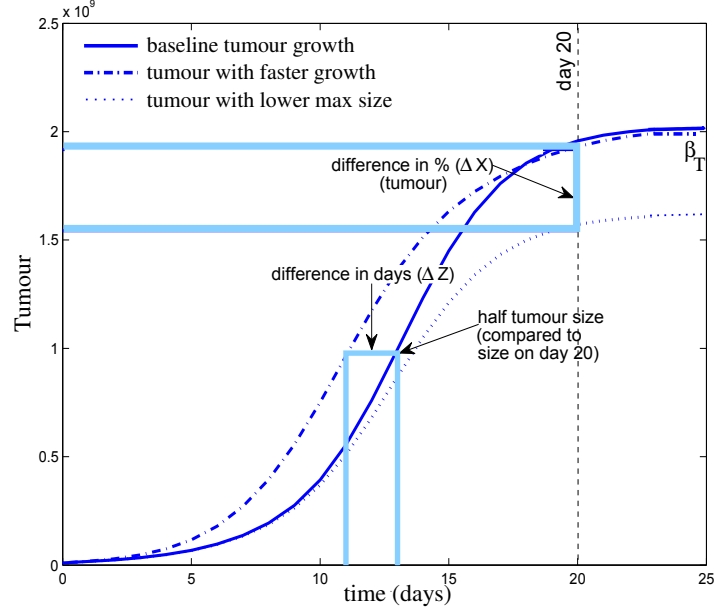


Figure 4: Dynamics of tumour growth for the baseline model (continuous curve) and two simulations showing faster tumour growth (dash-dot curve) and tumour growth with smaller maximum size (dotted curve), to exemplify how we calculate  $\Delta X$  and  $\Delta Z$ .  $\Delta X$  gives the percentage change in maximum tumour size, as model parameters are varied.  $\Delta Z$  gives the change in the number of days until the tumour reaches half the size obtained with the baseline model on day 20.

## 5. Sensitivity analysis

Even if we estimated some parameter values using tumour and macrophages data from [Chen et al. \(2011\)](#), other parameters values were guessed. To ensure that the general conclusions of the model are still valid if we change slightly the model parameters and the initial conditions of the simulations, we perform a local sensitivity analysis (where we change one value while keeping all other values fixed). This analysis also helps us identify the parameter space where we could see an improvement in cancer outcomes.

For the sensitivity analysis, we vary the initial conditions within the range shown in Table [A.4](#), the model parameters within the range shown in Table [A.6](#), and the ratio  $k = k_{12}/k_{21}$  within the range shown in Table [A.3](#).

For each baseline value  $q$  of model parameters and initial conditions (that generated the simulations in Figure [3](#) and which will be referred to

as the *baseline model*), we consider the effect of changing  $q$  to  $q + \Delta q$ , where  $\Delta q$  is either positive or negative. In particular, if  $q$  is a parameter value, then  $q$  is changed with 7 incremental steps  $\Delta q = 30\%q$  within the range  $(-80\%q, +190\%q)$  (see Table A.6). If  $q$  is an initial condition value, then  $q$  is changed with 6 incremental steps within the ranges shown in Table A.4. Finally, if  $q = k = k_{12}/k_{21}$ , then we change  $k_{12}$  and  $k_{21}$  simultaneously from  $4 \times 10^{-7}$  to  $4 \times 10^{-3}$  in 100 steps creating 10.000 simulations. However, to keep the results tractable, in Table A.3 we present the most informative 7-steps changes in the ratio  $k$ , with  $k_{12} \in (5 \times 10^{-5}, 2 \times 10^{-5})$  and  $k_{21} \in (4 \times 10^{-5}, 1.6 \times 10^{-5})$ .

The change from  $q$  to  $q + \Delta q$  leads to a change in the total tumour size  $x_T = x_{Ts} + x_{Tn}$  (see Figure 4). Denoting by  $X = x_T(20)$  the tumour size on day 20, as obtained with the baseline parameter values and initial conditions (see Figure 3A), then the change in  $q$  leads to a change from  $X$  to  $X + \Delta X$ , where  $\Delta X$  is the percentage change on day 20. We chose to focus on tumour size on day 20 since the experimental studies in Chen et al. (2011) show that the carrying capacity  $\beta_T = 2 \times 10^9$  cells (corresponding to a tumour volume of  $\approx 3\text{cm}^3$ ) is reached after 20 days. However, to ensure that the tumour is indeed at the carrying capacity and to investigate long term prognosis, we also investigate the percentage change in tumour population on day 50.

Moreover, many experimental studies investigate the effect of the ratio M2/M1 on tumour size, to test whether this ratio can be used as a biomarker for tumour development (Herwig et al., 2013). Therefore, we will use sensitivity analysis to quantify the relationship between the ratio M2/M1 at day 7 (for comparison with the data; see Figure 2) and the changes in the tumour population at days 20 and 50, as a result of varying  $k$  in the simulations.

While a decrease in the tumour might be the most desirable outcome, an increase in the number of days to reach a certain tumour size can extend the life expectancy. Therefore, we introduce a second value,  $Z$ , to represent the time the tumour grows to half the carrying capacity, i.e., to half the size obtained on day 20 with the baseline model (see Figure 4). Thus, a change from  $q$  to  $q + \Delta q$  will lead to a change from  $Z$  to  $Z + \Delta Z$ , which might not correlate with the change  $X$  to  $X + \Delta X$  (as shown in Figure 4). Note here that we refer to the growth until the tumour reaches half the carrying capacity as early tumour growth.

In the following subsections we show the change in the tumour size at days 20 & 50, and in the number of days to reach half the tumour size on day 20, when we vary the initial conditions (Section 5.1), the parameter values



317 (Section 5.2), the ratio  $k$  (Section 5.3) and the ratio M2/M1 (Section 5.4).

### 318 5.1. Sensitivity to initial conditions

319 Figure 5 shows that changing  $x_{Ts}(0)$  (within the interval shown in Table  
 320 A.4) has the greatest effect on the final tumour population (panel A), and on  
 321 the number of days to reach half of tumour size on day 20 (panel B). A change  
 322 in  $x_{Tn}(0)$  (within the interval shown in Table A.4) does not have a significant  
 323 effect, which is not surprising since these cells can grow uncontrolled by the  
 324 immune response. In regard to the change in the initial conditions for the  
 325 immune cells, only a change in  $x_{M2}(0)$  has some effect: (i) it can decrease  
 326 the total tumour size by  $-3\%$  or increase it by  $+4\%$  (Table A.4), or (ii) it  
 327 can decrease/increase by  $\mp 2$  the number of days until the tumour reaches  
 328 half the size obtained on day 20 with the baseline model (Table A.5).

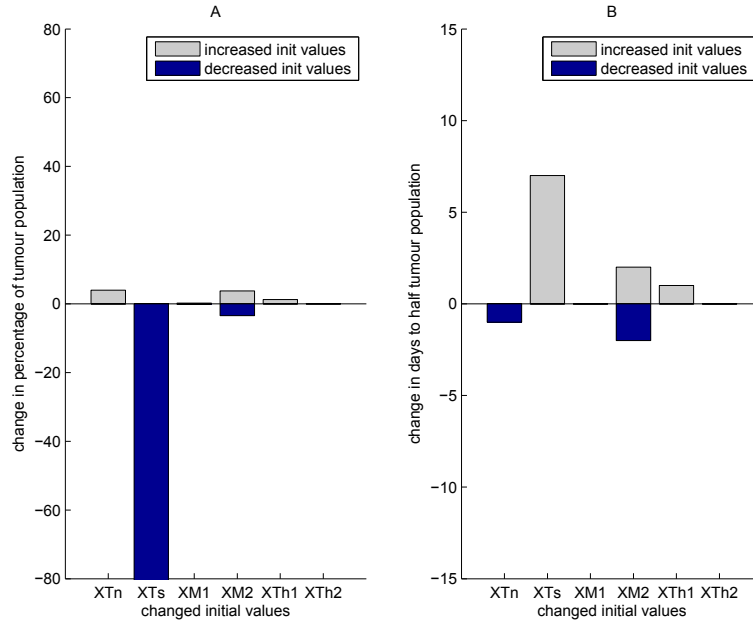


Figure 5: Change in tumour as a result of variation in initial conditions from the baseline values, as described in Tables A.4 and A.5. (A) Percentage of change from the baseline tumour population after 20 days of simulation (Table A.4). (B) Change in the number of days until the tumour reaches half the tumour size obtained in the baseline model on day 20 (Table A.5).

## 5.2. Sensitivity to parameters

Figure 6 shows the effect that varying model parameters has on the percentage change in the tumour size (panel A; see also Table A.6) and on the number of days to reach half the tumour size obtained on day 20 with the baseline model (panel B; see also Table A.7). As expected, the proliferation rate  $r$  and the carrying capacity  $\beta_T$  have the largest influence on the tumour population. However, it is unexpected that the re-polarisation rates  $k_{12}$  and  $k_{21}$  for the M2 and M1 macrophages, also have a large impact on tumour. These parameters appear in the steady states for  $x_{M1}$  and  $x_{M2}$ , and are involved in the ratio of M2/M1 macrophages. We will return to these rates in Section 5.3, when we will investigate in more detail the role of  $k = k_{12}/k_{21}$  on tumour growth.

Other parameters that influence tumour dynamics are:  $k_{sn}$ , the rate at which the  $x_{Ts}$  cells become  $x_{Tn}$  cells;  $\delta_{mn}$ , the rate at which  $x_{Tn}$  cells are eliminated by M1 macrophages;  $\delta_{ms}$ , the elimination rate of  $x_{Ts}$  tumour cells by the M1 macrophages;  $\delta_{m2}$ , the death rate of M2 cells. These results support the theory that both M1 and M2 cells influence tumour dynamics.

## 5.3. Sensitivity to the ratio $k = k_{12}/k_{21}$

In Figure 7A we show the percentage change from the baseline model, in tumour size on day 20 versus the ratio  $k = k_{12}/k_{21}$ . For  $k < 1$  the tumour is reduced by 40%, while for  $k > 1$  the changes in tumour at day 20 can vary from -40% to +5%, depending on the exact values of the rates  $k_{12}$  and  $k_{21}$ . In Figure 7B we show the percentage change in tumour size on day 50 versus  $k$ . In this case, for  $k \geq 1$  the tumours stay at their carrying capacity (i.e., no change from the value obtained with the baseline parameters). However, for  $k < 1$ , the tumour size on day 50 is reduced between 0-35%, again depending on the specific values of the macrophage re-polarisation rates  $k_{12}$  and  $k_{21}$ . We deduce from here that the ratio  $k = k_{12}/k_{21}$  is not a clear indicator of tumour dynamics; the particular values of  $k_{12}$  and  $k_{21}$  that lead to the same ratio  $k$  influence whether the tumour decreases or increases.

In Figure 8 we plot the time-dynamics of tumour population  $x_{Tn} + x_{Ts}$  for different values of  $k_{12}$  and  $k_{21}$  with the same ratio  $k$  ( $k = 3.3$  top panel;  $k = 1.2$  middle panel;  $k = 0.6$  bottom panel). The results clearly show that changing  $k_{12}$  and  $k_{21}$  while keeping  $k = k_{12}/k_{21}$  constant leads to different medium-term ( $0 < t < 25$ ) and long-term ( $t > 35$ ) tumour dynamics.

To understand better the role of  $k_{12}$  and  $k_{21}$  rates on tumour dynamics, in Figure 9 we graph the changes in tumour size and tumour growth versus

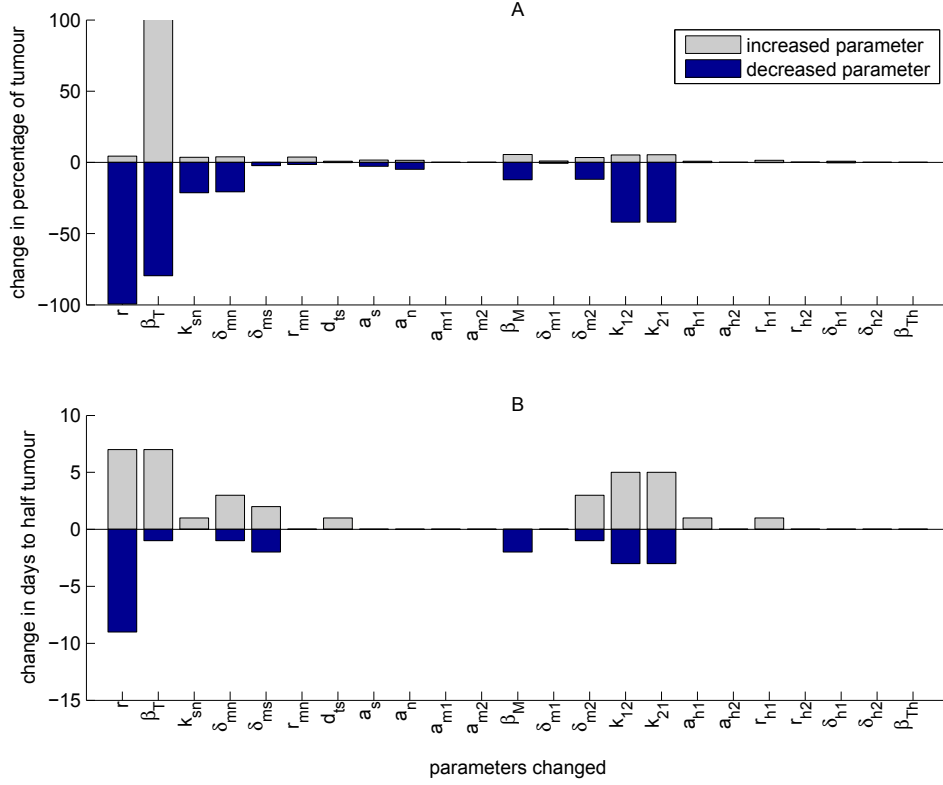


Figure 6: Change in tumour size, from the baseline model, as a result of the change in model parameters from -80% to +190% of their baseline values (shown in Tables A.6 and A.7.). (A) Percentage change of tumour size on day 20 (Table A.6). (B) Change in the number of days until tumour reaches half the tumour size observed on day 20 with the baseline model (Table A.7 ).

the difference  $k_{12} - k_{21}$ . When  $k_{12} - k_{21} \in (0, 1 \times 10^{-5})$ , there is an abrupt shift for the percentage change in tumour size at day 20 (see Figure 9A), leading to a reduction in tumour up to 42%. A similar shift, occurring for  $k_{12} - k_{21} \in (-2 \times 10^{-5}, 0)$ , can be observed also in the percentage change in tumour size at day 50 (see Figure 9B), although this is accompanied by a smaller reduction in tumour.

#### 5.4. Sensitivity to M2/M1 ratio

Changing the ratio  $k = k_{12}/k_{21}$  also leads to a change in the ratio of M2 and M1 macrophages:  $x_{M2}/x_{M1}$ . In Figure 10 we graph the time-dynamics

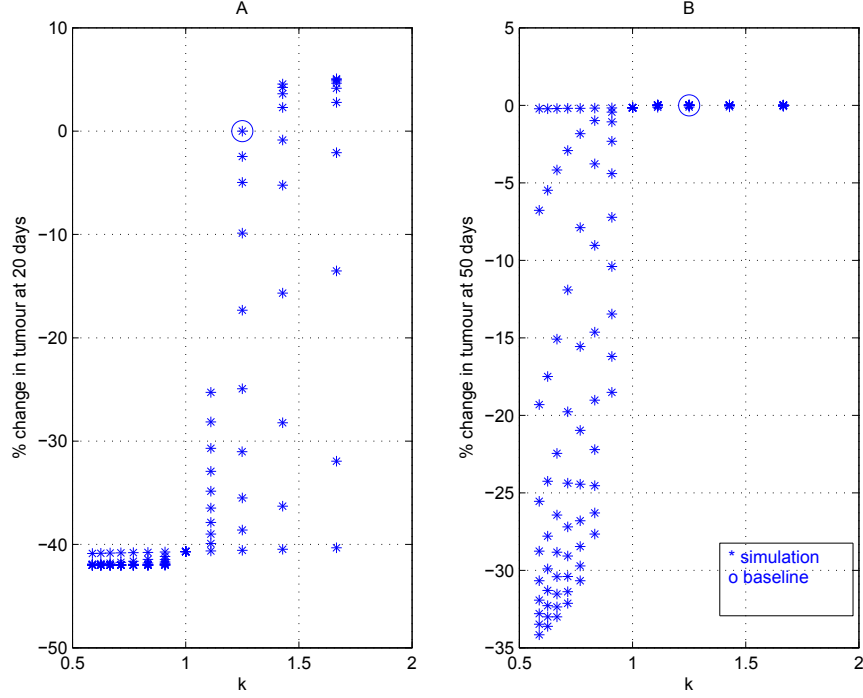


Figure 7: Percentage change from the baseline model (see the open circle for  $k = 1.2$ ) in: (A) tumour cells on day 20, and (B) tumour cells on day 50, for different values of the ratio  $k = k_{12}/k_{21}$  (as given by Table A.3). (A) For  $k > 1$ , tumour size on day 20 can increase or decrease depending on the actual values of  $k_{12}$  and  $k_{21}$ . For  $k < 1$ , tumour size on day 20 always decreases. (B) For  $k > 1$ , the tumours always reach the carrying capacity on day 50. For  $k < 1$  the tumours can be reduced in size by varying degrees, depending on the actual values of  $k_{12}$  and  $k_{21}$ .

375 of these macrophages for three different ratios of  $k$  ( $k = 3.3$  in top panel,  
 376  $k = 1.2$  in middle panel,  $k = 0.6$  in bottom panel). The dashed curves  
 377 show the baseline dynamics of M1 macrophages and the crosses show the  
 378 baseline dynamics of M2 macrophages (for the baseline  $k_{12}$  and  $k_{21}$  values; as  
 379 in Figure 3). The dashed-dotted and continuum curves show the dynamics  
 380 of M1 and M2 macrophages, respectively, for various  $k_{12}$  and  $k_{21}$  values that  
 381 lead to specific  $k$  ratios. In none of these cases is the tumour completely  
 382 eliminated; however the final tumour sizes approach different steady-state  
 383 values (as shown in Figure 8). This analysis indicates that the same ratio  
 384  $k$  can produce different M2/M1 profiles, with the shift between type-I and

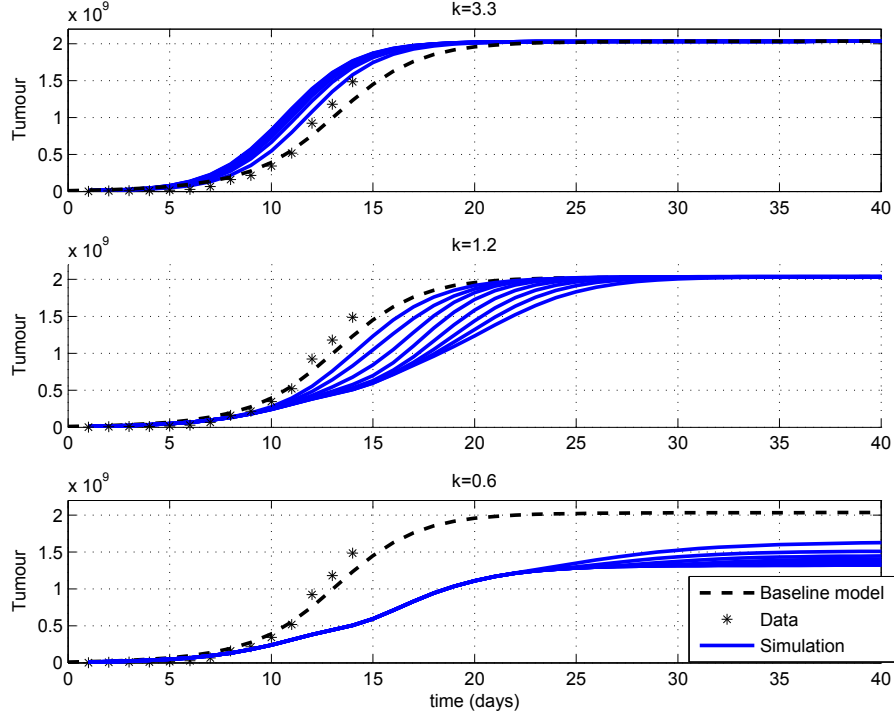


Figure 8: Change in tumour population, from the baseline model, as a result of the change in the ratio  $k = k_{12}/k_{21}$ . Simulations are performed by changing the values  $k_{12}$  and  $k_{21}$  for different ratios  $k$  ( $k = 3.3$ ,  $k = 0.6$ , and the baseline value  $k = 1.2$ ). Since different combinations of  $k_{12}$  and  $k_{21}$  result in the same ratio but with different tumour dynamics, it implies that the ratio  $k$  cannot be used to predict the tumour dynamics.

type-II immune responses occurring at different days. The change in the tumour dynamics is related to the day when the M2 cells outnumber the M1 cells.

In Figure 11 we show the ratio M2:M1 at day 7 and 14 (i.e.,  $x_{M2}(7)/x_{M1}(7)$  and  $x_{M2}(14)/x_{M1}(14)$ ) for different  $k$  values. For  $k < 1.2$  the dynamics on days 7&14 is dominated by the M1 macrophages. For  $k > 1.2$ , the dynamics on days 7&14 is dominated by the M2 macrophages. For  $k = 1.2$  (see the plots on the main diagonal), there are different percentages of M2 and M1 macrophages on day 7 and day 14, depending on the particular values of  $k_{12}$  and  $k_{21}$  used.

In Figure 12 we show the change in tumour size on day 20 (panel A) and

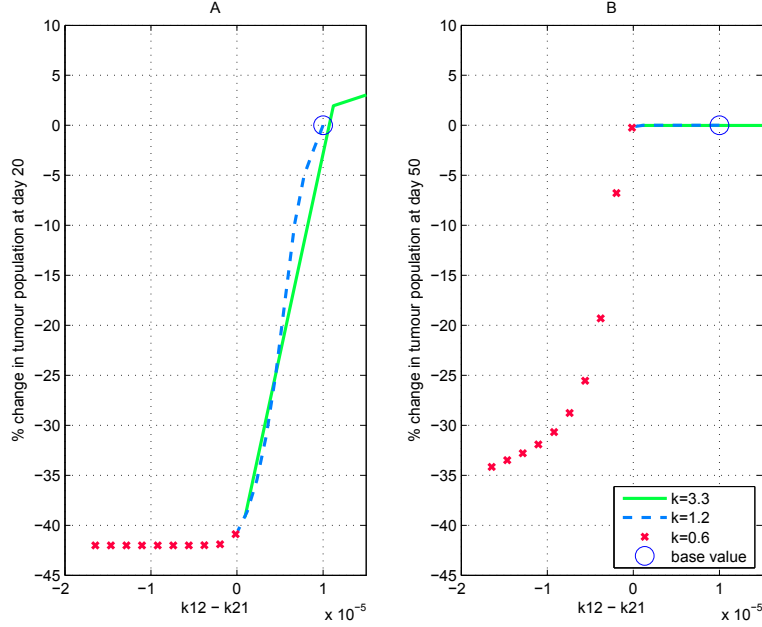


Figure 9: Percentage of change, from baseline value (open circle), in tumour size on day 20 (panel A) and on day 50 (panel B) when  $k_{12} - k_{21}$  is varied while keeping constant the ratio  $k = k_{12}/k_{21}$  ( $k = 3.3$  continuous curve,  $k = 1.2$  dashed curve,  $k = 0.6$  asterisk).

day 50 (panel B), as we vary  $k_{12}$  and  $k_{21}$  within the range shown in Table A.3, which then leads to a change in  $x_{M2}/x_{M1}$  at day 7. The results show that the tumour sizes on day 20 corresponding to  $x_{M2}(7)/x_{M1}(7) \leq 1$  are completely different from the tumour sizes corresponding to  $x_{M2}(7)/x_{M1}(7) > 1$ . Note here the lower median value for tumour size when  $x_{M2}/x_{M1} \leq 1$  compared to the case  $x_{M2}/x_{M1} > 1$ . These results persist also for the tumour sizes calculated at day 50, however, in this case the median value for tumour size when  $x_{M2}/x_{M1} \leq 1$  is slightly higher. This is consistent with the experimental results by Herwig et al. (2013), who classified melanoma in 2 different classes of tumour gene expression profiles based on the M2/M1 ratio (for a group of 20 patients).

## 6. Summary and Discussion

The role of M1 and M2 macrophages on tumour growth, and the use of M2/M1 ratio as an early-time marker for tumour prognosis, have attracted

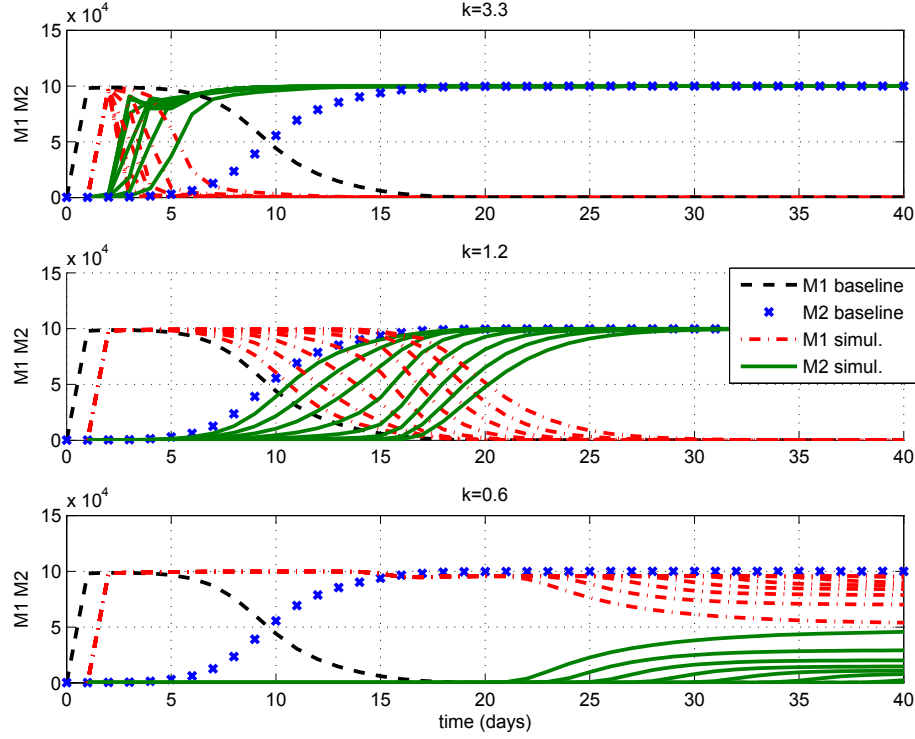


Figure 10: Time-dynamics of M1 and M2 macrophages for different values of  $k = k_{12}/k_{21}$ :  $k = 3.3$ ,  $k = 1.2$  (baseline ratio), and  $k = 0.6$ . In addition to showing the baseline dynamics of M1 and M2 macrophages, we also run simulations with multiple  $k_{12}$  and  $k_{21}$  values resulting in the same ratio. For  $k > 1$  the M2 macrophages dominate the dynamics, and the tumour reaches the carrying capacity (see also Fig. 8 top two panels). For  $k = 0.6$  the M1 macrophages dominate the dynamics, and the tumour is reduced below the carrying capacity (see also Fig. 8 bottom panel).

lots of interest over the last few years. Despite numerous experimental studies on the topic, we still lack a deeper understanding of the dynamics between the M1 and M2 macrophages and the tumour environment.

In this paper, we introduced a mathematical model that investigated the dynamics between the M1 and M2 macrophages, Th1 and Th2 immune cells, immunogenic and non-immunogenic tumour cells. We first focused on the steady states exhibited by this model and their stability. The results indicated that, when the tumour and immune cells were present, the steady states were not unique (see also Figure B.13B). The existence of multiple

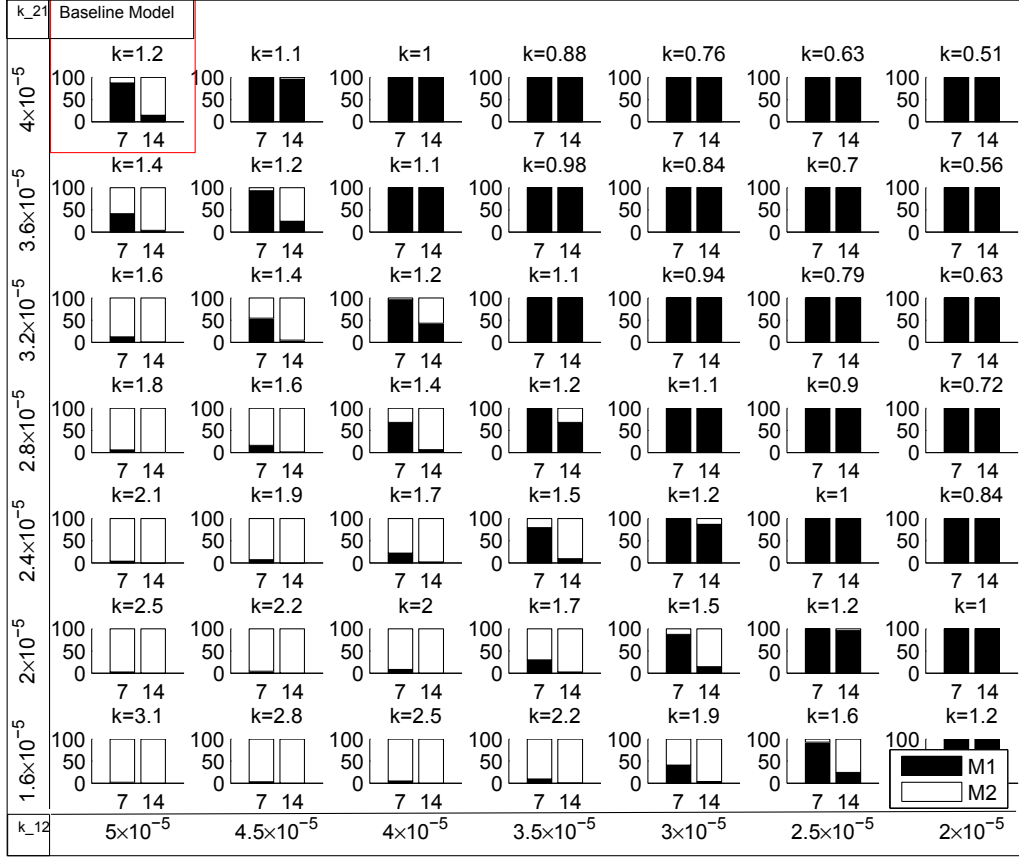


Figure 11: The percentage of M2&M1 macrophages on days 7 and 14, for different ratios of  $k = k_{12}/k_{21}$ . The ratio is shown above each small figure. Simulations are performed by changing  $k_{21}$  from  $4 \times 10^{-5}$  to  $1.6 \times 10^{-5}$  (see vertical axis) and  $k_{12}$  from  $5 \times 10^{-5}$  to  $2 \times 10^{-5}$  (see horizontal axis) in 7 steps.

states emphasised the complexity of the model dynamics, and the difficulty to understand analytically the role of the M2:M1 ratio on tumour persistence/elimination. Then, we performed an in-depth local sensitivity analysis to investigate the role of model parameters and of initial conditions on tumour outcome. Particular attention was paid to the role of  $k = k_{12}/k_{21}$  on the shift from a type-I immune response to a type-II immune response.

The sensitivity analysis allowed us to identify the parameter values that can lead to a slow-down in tumour growth or to smaller tumour sizes. In



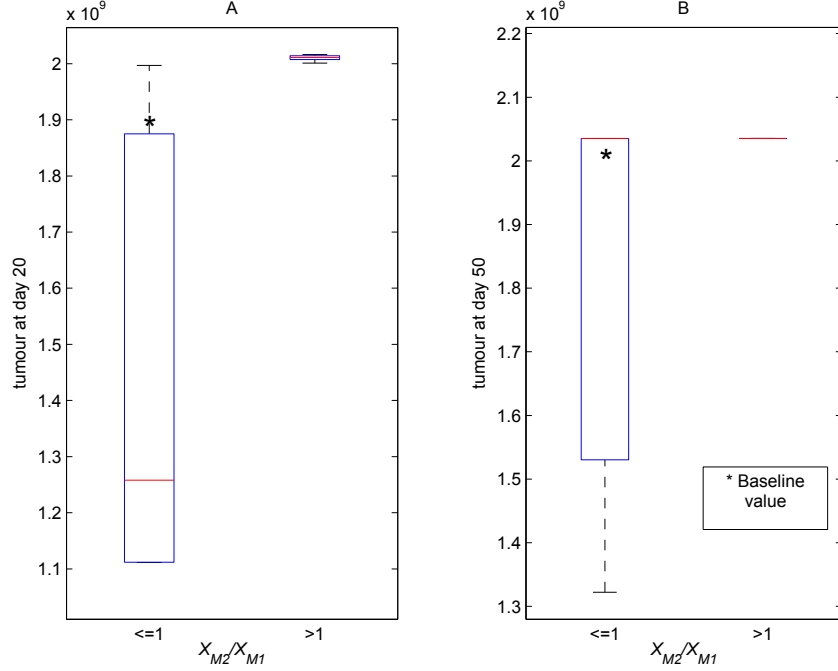


Figure 12: (A) Total tumour size on day 20, when the ratio of M2/M1 macrophages on day 7 is either  $x_{M2}(7)/x_{M1}(7) > 1$  or  $x_{M2}(7)/x_{M1}(7) \leq 1$ , as a result of varying  $k_{21} \in (1.6 \times 10^{-5}, 4 \times 10^{-5})$  and  $k_{12} \in (2 \times 10^{-5}, 5 \times 10^{-5})$  in 7 steps. (B) Total tumour size on day 50, for  $x_{M2}(7)/x_{M1}(7) > 1$  and  $x_{M2}(7)/x_{M1}(7) \leq 1$ , as a result of varying  $k_{21} \in (1.6 \times 10^{-5}, 4 \times 10^{-5})$  and  $k_{12} \in (2 \times 10^{-5}, 5 \times 10^{-5})$  in 7 steps.

addition to the expected importance of tumour growth rate  $r$  and tumour carrying capacity  $\beta_T$  on overall tumour dynamics, two other parameters,  $k_{12}$  and  $k_{21}$ , showed unexpected impact on tumour growth and decay (see Figures 6, 10). Moreover, we showed that while the ratio  $k = k_{12}/k_{21}$  is important in predicting long-term tumour control or growth to the carrying capacity, the exact tumour sizes are given by the particular values of the re-polarisation rates  $k_{12}$  and  $k_{21}$  (Figures 7-10). In addition, the rates  $k_{12}$  and  $k_{21}$  influenced the day of the shift from a type-I to a type-II immune response (and subsequent tumour growth); see Figure 10.

The results explain the importance of role of the M2:M1 ratio on tumour progression and prognosis. While in environments with M2:M1 ratio  $> 1$  the tumour will grow to the carrying capacity (Figure 12), in environments

439 with M2:M1 ratio  $< 1$  the tumour growth can not be predicted with the  
440 macrophage and re-polarisation ratios  $k$  alone and also depends on the values  
441 of the re-polarisation rates (Figure 9).

442 We emphasise that the results of our study were based on available data  
443 from mice experiments. However, even if mouse models have been used  
444 widely to study the interactions between the immune system and cancer to  
445 propose hypotheses in regard to human cancers, it is possible that data from  
446 human clinical trials (still scarce at this moment) would lead to different  
447 results. Nevertheless, it was not the goal of our study to compare the results  
448 for mouse and human data sets. Rather, our study focused on investigating  
449 the role of ratio of M1 and M2 macrophages as a marker for tumour prognosis  
450 in mouse models. As mentioned before, we showed that the ratio of mouse  
451 macrophage populations can be a suitable predictor of tumour outcome if  
452 M2/M1  $> 1$  in early tumour stages, i.e., before the tumour reaches half  
453 the carrying capacity (in Figure 12 we focused on the value of this ratio at  
454 day 7). If these results can be confirmed also for human data, then they  
455 can have implications to human treatment protocols, since clinicians could  
456 use the ratio M2/M1  $> 1$  as a biomarker for decisions regarding various  
457 long-term patient treatments. Moreover, the possibility of re-programming  
458 the environment towards a M1 phenotype (as suggested, for example, by  
459 Heusinkveld and van der Burg (2011); Tang et al. (2013)), could also impact  
460 positively the outcome of cancer treatments, by creating the possibility of  
461 a reduced long-term tumour burden that can be further reduced with other  
462 types of treatment (e.g., combinations of immune therapies, viral therapies  
463 and/or chemotherapies).

464 To understand better the molecular-level mechanisms that control the  
465 dynamics of M1 and M2 cells, and their interactions with the tumour cells  
466 (with the purpose of designing treatments that would re-program the M2  
467 macrophages to a M1-phenotype) it is necessary to add more detail to the  
468 model (1). Further investigation should focus on the role of molecular-level  
469 dynamics (i.e., the pro- and anti-tumour cytokines produced by both Th cells  
470 and macrophages) on the pro-tumour and anti-tumour immune responses.

471 Finally, we stress that the model introduced in this article has a number  
472 of limitations. First, as mentioned before, the results of the model are valid  
473 only for mouse data. While it would be interesting to parametrise the model  
474 also for human data (to test the validity of these results in the context of hu-  
475 man clinical trials), such an investigation is beyond the scope of the current  
476 study. Second, we focused only on the non-spatial dynamics of tumour and

immune cells. However, tumours are highly heterogeneous and the immune cells might be localised in particular regions of the tumour. For example, the tumour-associated macrophages are usually found in the perivascular and cortical regions of the tumour, where they contribute to tumour growth and invasion (Carmona-Fontaine et al., 2013). In general, the mechanisms of immune cells localisations in particular areas of the tumours are still quite poorly understood, and future studies are necessary to understand the potential for new therapeutic avenues based on influencing this spatial localisation of immune cells. Last but not the least, the complex interactions between the tumour and immune cells give rise to highly nonlinear dynamics, which cannot be fully understood only via steady-state analysis, numerical simulations and sensitivity analysis. Nonlinear analysis and bifurcation theory should be used in the future to shed light on the observed dynamics.

## Acknowledgments

N.dB. acknowledges support from the BIOMICS project (EU FP7 Grant No. 318202). R.E. acknowledges support from an Engineering and Physical Sciences Research Council (UK) grant number EP/K033689/1 and a Northern Research Partnership (Scotland) grant.

## Appendix A. Summary of model parameters and variables

Table A.1 summarises the variables used in model (1), together with their initial values (i.e., the initial conditions for the simulations) and the ranges within which we varied these initial values for the local sensitivity analysis. Table A.2 summarises the parameters used throughout this paper, along with their values and units. Next, we describe how we estimated some of the parameters in Table A.2.

### *Parameter estimation.*

- To approximate the tumour growth rate  $r$ , we fit equation (1a) with no immune response to the melanoma growth data from Chen et al. (2011). We thus obtain  $r = 0.565$  cells/day, in line with the values reported by Eikenberry et al. (2009) (see Fig 2A).
- Most experimental studies euthanise the mice when the tumour reaches 2-3 cm<sup>3</sup>. In Chen et al. (2011), the tumour reached a volume of  $\approx 3$

Table A.1: Summary of variables used in the model, the baseline initial conditions (IC) and the range of IC used for the local sensitivity analysis.

States	Description	Baseline IC	Range IC
$x_{T_n}$	Density of non-immunogenic tumour cells	$10^3$	$(1, 10^7)$
$x_{T_s}$	Density of immunogenic tumour cells	$10^6$	$(1, 10^7)$
$x_{M1}$	Density of M1 macrophages	100	$(10, 10^4)$
$x_{M2}$	Density of M2 macrophages	100	$(10, 10^4)$
$x_{Th1}$	Density of Th1 helper cells	0	$(0, 10^5)$
$x_{Th2}$	Density of Th2 helper cells	0	$(0, 10^5)$

cm<sup>3</sup> on day 14. Therefore, we choose the carrying capacity for the tumour to be  $\beta_T = 2 \times 10^9$  (on the same order of magnitude as other theoretical studies; see [Eftimie et al. \(2010\)](#)).

- To calculate the death rate  $\delta_x$  of various cells, we use the formula  $t_{1/2} = \ln(2)/\delta_x$ , where  $t_{1/2}$  is their half-life. The half-life of mouse circulating blood monocytes, the precursor of macrophages, varies from about 17.4hr ([Van Furth, 1989](#); [Kuroda, 2010](#)) to 5 days ([Ginhoux and Jung, 2014](#)). For macrophages, we assume an average half-life of 3 days and calculate  $\delta_{m1,m2} = \ln(2)/3 \approx 0.23$  (similar to the value in [Wang et al. \(2012\)](#)). In regard to the effector CD4<sup>+</sup> T cells, about 90% of cells dies within the 7-14 days of the contraction phase ([Pepper and Jenkins, 2011](#)). Therefore we calculate  $\delta_{h1,h2} \in (\ln(2)/14, \ln(2)/7) \approx (0.049, 0.099)$ . Throughout this article, we choose  $\delta_{h1,h2} = 0.05$ .
- Experimental results in [Chen et al. \(2011\)](#) have shown that on day 7 there were only 15% M2 macrophages, while on day 14 this percentage increased to 85% M2 macrophages. We use these values to fit  $k_{12}$ , the rate at which M1 macrophages become M2, and  $k_{21}$ , the rate at which M2 macrophages become M1 (see Figure 2C),  $r_{mn}$  the proliferation rate of  $x_{T_n}$  cells in the presence of M2 macrophages, and  $\beta_M$  the carrying capacity of macrophages.
- The metastatic mouse melanoma tumour cells have a very high mutation rate compared to other tumour lines ([Cillo et al., 1987](#)). For example, the B16F10 melanoma cells have a rate of generation of drug-resistant clones of at least  $10^{-5}$ / cell/generation ([Cillo et al., 1987](#); [Hill et al., 1984](#)), while lower metastatic tumours can have a muta-

Table A.2: Summary and description of parameters that appear in model (1). Parameters are estimated by fitting model (1) to the experimental data from (Chen et al., 2011) and data from other experimental papers - as described in the *Parameter estimation* section in Appendix A, or they are sourced directly from the existent mathematical literature - indicated by a “\*”.

Param.	Value	Units	Description	Reference
$r$	0.565	$\text{day}^{-1}$	proliferation rate of tumour cells	(Chen et al., 2011)
$\beta_T$	$2 \times 10^9$	cells	carrying capacity of tumour cells	(Chen et al., 2011)
$k_{sn}$	0.1	$\text{day}^{-1}$	rate at which $x_{Ts}$ become $x_{Tn}$	guess
$\delta_{mn}$	$2 \times 10^{-6}$	$(\text{day cells})^{-1}$	killing rate of $x_{Tn}$ by $x_{M1}$	(Baba et al., 2008)
$\delta_{ms}$	$2 \times 10^{-6}$	$(\text{day cells})^{-1}$	killing rate of $x_{Ts}$ by $x_{M1}$	(Baba et al., 2008)
$r_{mn}$	$1 \times 10^{-7}$	$(\text{day cells})^{-1}$	proliferation rate of $x_{Tn}$ cells in the presence of $x_{M2}$ cells	guess
$\delta_{ts}$	$5.3 \times 10^{-8}$	$(\text{day cells})^{-1}$	killing rate of $x_{Ts}$ by $x_{Th1}$	(Hung et al., 1998)
$a_s$	$1 \times 10^{-6}$	$(\text{day cells})^{-1}$	activation rate of $x_{M1}$ triggered by $x_{Ts}$ antigens	guess
$a_n$	$5 \times 10^{-8}$	$(\text{day cells})^{-1}$	activation rate of $x_{M2}$ mediated by cytokines and growth factors produced by $x_{Tn}$	guess
$a_{m1}$	$5 \times 10^{-8}$	$(\text{day cells})^{-1}$	activation rate of $x_{M1}$ by type-I cytokines produced by $x_{Th1}$	guess
$a_{m2}$	$5 \times 10^{-8}$	$(\text{day cells})^{-1}$	activation rate of $x_{M2}$ by type-II cytokines produced by $x_{Th2}$	guess
$\beta_M$	$1 \times 10^5$	cells	carrying capacity of M1,M2 cells	guess
$\delta_{m1}$	0.2	$\text{day}^{-1}$	death rate of $x_{M1}$ cells	(Wang et al., 2012)*
$\delta_{m2}$	0.2	$\text{day}^{-1}$	death rate of $x_{M2}$ cells	(Wang et al., 2012)*
$k_{12}$	$5 \times 10^{-5}$	$(\text{day cells})^{-1}$	rate at which $x_{M1}$ become $x_{M2}$	(Chen et al., 2011)
$k_{21}$	$4 \times 10^{-5}$	$(\text{day cells})^{-1}$	rate at which $x_{M2}$ become $x_{M1}$	(Chen et al., 2011)
$a_{h1}$	$8 \times 10^{-3}$	$\text{day}^{-1}$	activation rate of $x_{Th1}$ by type-I cytokines produced by $x_{M1}$	(Ribeiro et al., 2002)*
$a_{h2}$	$8 \times 10^{-3}$	$\text{day}^{-1}$	activation rate of $x_{Th2}$ by type-II cytokines produced by $x_{M2}$	(Ribeiro et al., 2002)*
$r_{h1}$	$9 \times 10^{-6}$	$(\text{day cells})^{-1}$	proliferation rate of $x_{Th1}$ in the presence of type-I cytokines produced by $x_{M1}$ cells	guess
$r_{h2}$	$9 \times 10^{-6}$	$(\text{day cells})^{-1}$	proliferation rate of $x_{Th2}$ in the presence of type-II cytokines produced by $x_{M2}$ cells	guess
$\delta_{h1}$	0.05	$\text{day}^{-1}$	natural death rate of $x_{Th1}$ cells	(Pepper and Jenkins, 2011)
$\delta_{h2}$	0.05	$\text{day}^{-1}$	natural death rate of $x_{Th2}$ cells	(Pepper and Jenkins, 2011)
$\beta_{Th}$	$1 \times 10^8$	cells	carrying capacity of Th cells	guess

tion rate of  $\approx 10^{-7}$ / cell/generation (Mareel et al., 1991). To model these high melanoma mutation rates, we assume an average growing cell population of  $\approx 10^4$  cells/generation, a 1-day generation of cells (since the doubling time is about 1.2 days), and take the mutation rate  $k_{sn} = 10^{-5}$ /cell/day  $\times 10^4$ cells = 0.1/day.

- To approximate the maximum rate at which the effector cells kill the tumour cells (at an effector:target ratio of 1:1), we use the following formula (where we ignore the proliferation of tumour cells, since we assume that cells do not proliferate anymore *in vitro*):

$$\frac{dT}{dt} = -\delta_{kill}TE, \quad (\text{A.1})$$

with  $T$  describing the target cells ( $T = x_{Tn}$  or  $T = x_{Ts}$ ) and  $E$  describing the effector cells ( $E = x_{M1}$  or  $E = x_{Th1}$ ). To approximate  $\delta_{kill}$  for macrophages (i.e.,  $\delta_{kill} = \delta_{ms} = \delta_{mn}$ ), we note that Baba et al. (2008) incubated for 18 hours  $CD4^+CD8^+$  macrophages of M1 phenotype with four different tumour cell lines. The killing of tumour cells reached maximum rate at an effector:target ratio of 30:1 (i.e.,  $1.2 \times 10^6$  effector cells and  $4 \times 10^4$  target cells). Moreover, the percent specific lysis varied between 10%-97%. Integrating equation (A.1) with respect to time from  $t = 0$  hrs to  $t_i = 18$  hrs, replacing  $E$  with  $E = 30T$  (for an effector:target ratio of 30), and assuming that the total number of target cells at the end of the incubation time  $t_i$  is  $T(t_i) = 100 - \%Lysis$ , we obtain

$$\delta_{kill} = \frac{\%Lysis}{T(0)(100 - \%Lysis)30t_i}. \quad (\text{A.2})$$

Therefore, for  $t_i = 18$  hrs = 0.75 days and  $T(0) = 4 \times 10^4$ cells, we obtain

$$\delta_{kill} = 3.6 \times 10^{-5}, \text{ for } \%Lysis=97\%, \quad (\text{A.3})$$

$$\delta_{kill} = 1.2 \times 10^{-7}, \text{ for } \%Lysis=10\%. \quad (\text{A.4})$$

For the purpose of this article, we will consider  $\delta_{mn} = \delta_{ms} = 2 \times 10^{-6}$ , corresponding to an average tumour  $\%Lysis = 65\%$ .

Finally, to approximate  $\delta_{kill}$  for Th1 cells (i.e.,  $\delta_{kill} = \delta_{ts}$ ), we note that Hung et al. (1998) incubated  $10^6$  B16 tumour cells with CD4 T cells. The maximum  $\%Lysis$  was 30%, and was obtained at an effector:target

ratio of about 32:1. Using again (A.1), and the assumption that cells were incubated for about 6 hours (=0.25 days), we obtain a killing rate

$$\delta_{kill} = \delta_{ts} = 5.3 \times 10^{-8}. \quad (\text{A.5})$$

Next, we introduce Tables A.3-A.7 that contain the values of parameters and initial conditions used for the sensitivity analysis in Section 5.

Table A.3: Changes in the ratio  $k = k_{12}/k_{21}$  for the sensitivity analysis.  $k_{12}$  is changed from  $5 \times 10^{-5}$  to  $2 \times 10^{-5}$ , and  $k_{21}$  is changed from  $4 \times 10^{-5}$  to  $1.6 \times 10^{-5}$  in 7 steps.

$k_{21}$	$k$	$k$	$k$	$k$	$k$	$k$	$k$
$4 \times 10^{-5}$	1.2	1.1	1	0.88	0.75	0.63	0.51
$3.6 \times 10^{-5}$	1.4	1.2	1.1	0.98	0.84	0.7	0.56
$3.2 \times 10^{-5}$	1.6	1.4	1.2	1.1	0.94	0.79	0.63
$2.8 \times 10^{-5}$	1.8	1.6	1.4	1.2	1.1	0.9	0.72
$2.4 \times 10^{-5}$	2.1	1.9	1.7	1.5	1.2	1	0.84
$2 \times 10^{-5}$	2.5	2.2	2	1.7	1.5	1.2	1
$1.6 \times 10^{-5}$	3.1	2.8	2.5	2.2	1.9	1.6	1.2
$k_{12}$	$5 \times 10^{-5}$	$4.5 \times 10^{-5}$	$4 \times 10^{-5}$	$3.5 \times 10^{-5}$	$3 \times 10^{-5}$	$2.5 \times 10^{-5}$	$2 \times 10^{-5}$

Table A.4: Percentage change in tumour size on day 20 (columns 4&6), for simulations with different initial conditions (IC). Columns 1&2 show the baseline values for the IC and the range within which they are varied. Columns 3&5 show the initial conditions that lead to a maximum *decrease/increase* in tumour size on day 20.

IC baseline value	Range for IC	IC for max tumour decrease	Max % <i>decrease</i> in tumour	IC for max tumour increase	Max % <i>increase</i> in tumour
$x_{Tn}(0) = 10^3$	$(1, 10^7)$	1	0 %	$10^7$	4 %
$x_{Ts}(0) = 10^6$	$(1, 10^7)$	1	-98 %	$10^7$	0 %
$x_{M1}(0) = 10^2$	$(10, 10^4)$	10	0 %	$10^4$	0 %
$x_{M2}(0) = 10^2$	$(10, 10^4)$	10	-3 %	$10^4$	4 %
$x_{Th1}(0) = 0$	$(0, 10^5)$	0	0 %	$3 \times 10^4$	1 %
$x_{Th2}(0) = 0$	$(0, 10^5)$	0	0 %	$10^5$	0 %

## Appendix B. Number of steady states

To investigate the number of TF1IP states, we substitute  $x_{Th1}^*$  given by (2) into the expression for  $x_{M1}^*$  (given by the same equation), which leads to

Table A.5: Maximum increase/decrease in the number of days to reach half the tumour population obtained on day 20 with the baseline model (see also Figure 4), as we vary the initial conditions (IC). Columns 1&2 show the baseline values for the IC and the range within which they are varied. Columns 3&5 show the initial conditions that lead to a maximum *decrease/increase* in the number of days to reach half the tumour population on day 20.

Baseline IC value	Range for IC	IC for max time <i>decrease</i>	Max <i>decrease</i> in nbr. days	IC for max time <i>increase</i>	Max <i>increase</i> in nbr. days
$x_{Tn} = 10^3$	$(1, 10^7)$	$5 \times 10^6$	-1 days	1	0 days
$x_{Ts} = 10^6$	$(1, 10^7)$	$10^7$	0 days	1	7 days
$x_{M1} = 100$	$(10, 10^4)$	10	0 days	10	0 days
$x_{M2} = 100$	$(10, 10^4)$	5010	-2 days	10	2 days
$x_{Th1} = 0$	$(0, 10^5)$	0	0 days	$10^4$	0 days
$x_{Th2} = 0$	$(0, 10^5)$	0	0 days	0	0 days

$$A_1(x_{Th1}^*)^3 + B_1(x_{Th1}^*)^2 + C_1(x_{Th1}^*) + D_1 = 0, \quad (\text{B.1})$$

where

$$A_1 = -\frac{a_{m1}r_{h1}\beta_M}{\beta_{Th}}, \quad B_1 = a_{m1}\beta_M r_{h1} - a_{m1}\delta_{h1} + \frac{\delta_{m1}\beta_M r_{h1}}{\beta_{Th}}, \quad (\text{B.2a})$$

$$C_1 = a_{m1}\beta_M a_{h1} - \delta_{m1}\beta_M r_{h1}, \quad D_1 = -\delta_{m1}\beta_M a_{h1}. \quad (\text{B.2b})$$

568 This equation has a unique real solution (for the parameter values given in  
569 Table A.2), and hence there is a unique TF1IP steady state.

570 Similarly, we can investigate the number of TF2IP states by substituting  
571  $x_{Th2}^*$  given by (3) into the expression for  $x_{M2}^*$  (also given by (3)), which leads  
572 to a cubic equation similar to (B.1). Since this cubic equation has a unique  
573 solution, we deduce that also the TF2IP state is unique.

574 Due to the complexity of the TFIP states, we can investigate their unique-  
575 ness only numerically. In Figure B.13(a) we show that the solution curves of  
576 (4) intersect for an infinite number of values, and thus system (1) can have  
577 an infinite number of steady states.

578 To investigate the number of TP1IP states, note that in (5) neither  $x_{M1}^*$   
579 nor  $x_{Th}^*$  are affected by  $x_{Tn}^*$  ( $x_{M1}^*$  is influenced only by  $x_{Ts}^* = 0$ ). Thus the  
580 states  $x_{M1}^*$  and  $x_{Th1}^*$  in (5) are also solutions of equation (B.1), and they are  
581 unique. Similarly, the TP2IP state is unique (which can be checked easily by  
582 substituting (6b) into (6a)). As discussed in Appendix C, this state is stable.



Table A.6: Percentage of change in tumour size on day 20 (columns 4&6), for simulations with different parameter values. Columns 1&2 show the baseline values of parameters that appear in model (1) and the range within which they are varied. Columns 3&5 show the parameter values that lead to the max *decrease/increase* in tumour population on day 20.

Baseline param. values	Simulation range	Param. for max % <i>decrease</i>	Max % <i>decrease</i> tumour size	Param. for max % <i>increase</i>	Max % <i>increase</i> tumour size
$r = 0.565$	(0.113, 1.6385)	0.113	-99	1.638	4
$\beta_T = 2 \times 10^9$	$(4 \times 10^8, 5.8 \times 10^9)$	$4 \times 10^8$	-80	$5.8 \times 10^9$	175
$k_{sn} = 0.1$	(0.02, 0.29)	0.02	-21	0.29	4
$\delta_{mn} = 2 \times 10^{-6}$	$(4 \times 10^{-7}, 5.8 \times 10^{-6})$	$5.8 \times 10^{-6}$	-21	$4 \times 10^{-7}$	4
$\delta_{ms} = 2 \times 10^{-6}$	$(4 \times 10^{-7}, 5.8 \times 10^{-6})$	$5.8 \times 10^{-6}$	-2	$2.2 \times 10^{-6}$	0
$r_{mn} = 1 \times 10^{-7}$	$(2 \times 10^{-8}, 2.9 \times 10^{-7})$	$2 \times 10^{-8}$	-2	$2.9 \times 10^{-7}$	4
$\delta_{ts} = 5.3 \times 10^{-8}$	$(1.06 \times 10^{-8}, 1.53 \times 10^{-7})$	$9.01 \times 10^{-8}$	0	$1.06 \times 10^{-8}$	1
$a_s = 1 \times 10^{-6}$	$(2 \times 10^{-7}, 2.9 \times 10^{-6})$	$2.90 \times 10^{-6}$	-3	$2 \times 10^{-7}$	2
$a_n = 5 \times 10^{-8}$	$(1 \times 10^{-8}, 1.45 \times 10^{-8})$	$1 \times 10^{-8}$	-5	$1.45 \times 10^{-7}$	1
$a_{m1} = 5 \times 10^{-8}$	$(1 \times 10^{-8}, 1.45 \times 10^{-8})$	$1.45 \times 10^{-7}$	0	$1 \times 10^{-8}$	0
$a_{m2} = 5 \times 10^{-8}$	$(1 \times 10^{-8}, 1.45 \times 10^{-8})$	$1 \times 10^{-8}$	0	$1.45 \times 10^{-7}$	0
$\beta_M = 1 \times 10^5$	$(2 \times 10^4, 2.9 \times 10^5)$	$5 \times 10^4$	-12	$2.9 \times 10^5$	6
$\delta_{m1} = 0.2$	(0.04, 0.58)	0.04	-1	$5.8 \times 10^{-1}$	1
$\delta_{m2} = 0.2$	(0.04, 0.58)	0.58	-12	$4 \times 10^{-2}$	3
$k_{12} = 5 \times 10^{-5}$	$(1 \times 10^{-5}, 1.5 \times 10^{-4})$	$2.5 \times 10^{-5}$	-42	$1.45 \times 10^{-5}$	5
$k_{21} = 4 \times 10^{-5}$	$(8 \times 10^{-6}, 1.16 \times 10^{-5})$	$6.8 \times 10^{-5}$	-42	$8 \times 10^{-6}$	5
$a_{h1} = 8 \times 10^{-3}$	$(1.6 \times 10^{-3}, 2.32 \times 10^{-3})$	$1.36 \times 10^{-2}$	0	$1.6 \times 10^{-3}$	1
$a_{h2} = 8 \times 10^{-3}$	$(1.6 \times 10^{-3}, 2.32 \times 10^{-3})$	$1.6 \times 10^{-3}$	0	$2.32 \times 10^{-2}$	0
$r_{h1} = 9 \times 10^{-6}$	$(1.8 \times 10^{-7}, 2.61 \times 10^{-5})$	$9.9 \times 10^{-6}$	0	$1.53 \times 10^{-5}$	1
$r_{h2} = 9 \times 10^{-6}$	$(1.8 \times 10^{-7}, 2.61 \times 10^{-5})$	$1.8 \times 10^{-6}$	0	$2.61 \times 10^{-5}$	0
$\delta_{h1} = 0.05$	(0.01, 0.145)	0.01	0	0.145	1
$\delta_{h2} = 0.05$	(0.01, 0.145)	0.07	0	0.115	0
$\beta_{Th} = 1 \times 10^8$	$(2 \times 10^7, 2.9 \times 10^8)$	$2.9 \times 10^8$	0	$2 \times 10^7$	0

583 Finally, the number of TPIP states is investigated graphically in Figure  
584 B.13(B). Note that the surface curves given by the right-hand-side of equa-  
585 tions (1a), (1c) and (1d) (obtained after we substitute into these equations  
586 the values of  $x_{M1}^*$  and  $x_{M2}^*$  calculated from (1e)-(1f)), intersect for an infinite  
587 number of  $x_{Tn}^*$  values. Therefore, there is an infinite number of TPIP states.

## 588 AppendixC. Jacobian matrix

589 The Jacobian matrix associated with system (1) is given by:

Table A.7: Maximum *decrease/increase* in number of days (columns 4&6) to reach half the tumour size obtained on day 20 with the baseline model. Columns 1&2 show the baseline values of parameters that appear in model (1) and the range within which they are varied. Columns 3&5 show the parameter values that lead to the max *decrease/increase* in the number of days to reach half the tumour population obtained on day 20 with the baseline parameter values.

Baseline param. values	Simulation range	Param. value for max <i>decrease</i>	<i>Decrease</i> in nbr. days	Param. value for max <i>increase</i>	<i>Increase</i> in nbr. days
$r = 0.565$	(0.113, 1.6385)	1.63	-9	0.113	7
$\beta_T = 2 \times 10^9$	$(4 \times 10^8, 5.8 \times 10^9)$	$4 \times 10^9$	-1	$4 \times 10^8$	7
$k_{sn} = 0.1$	(0.02, 0.29)	0.08	0	0.02	1
$\delta_{mn} = 2 \times 10^{-6}$	$(4 \times 10^{-7}, 5.8 \times 10^{-6})$	$4 \times 10^{-7}$	-1	$5.8 \times 10^{-6}$	3
$\delta_{ms} = 2 \times 10^{-6}$	$(4 \times 10^{-7}, 5.8 \times 10^{-6})$	$4 \times 10^{-7}$	-2	$4 \times 10^{-6}$	2
$r_{mn} = 1 \times 10^{-7}$	$(2 \times 10^{-8}, 2.9 \times 10^{-7})$	$2 \times 10^{-8}$	0	$2 \times 10^{-8}$	0
$\delta_{ts} = 5.3 \times 10^{-8}$	$(1.06 \times 10^{-8}, 1.53 \times 10^{-7})$	$1.06 \times 10^{-8}$	0	$1.06 \times 10^{-7}$	1
$a_s = 1 \times 10^{-6}$	$(2 \times 10^{-7}, 2.9 \times 10^{-6})$	$2 \times 10^{-7}$	0	$2 \times 10^{-7}$	0
$a_n = 5 \times 10^{-8}$	$(1 \times 10^{-8}, 1.45 \times 10^{-8})$	$1 \times 10^{-8}$	0	$1 \times 10^{-8}$	0
$a_{m1} = 5 \times 10^{-8}$	$(1 \times 10^{-8}, 1.45 \times 10^{-8})$	$1 \times 10^{-8}$	0	$1 \times 10^{-8}$	0
$a_{m2} = 5 \times 10^{-8}$	$(1 \times 10^{-8}, 1.45 \times 10^{-8})$	$1 \times 10^{-8}$	0	$1 \times 10^{-8}$	0
$\beta_M = 1 \times 10^5$	$(2 \times 10^4, 2.9 \times 10^5)$	$2 \times 10^4$	-2	$8 \times 10^4$	0
$\delta_{m1} = 0.2$	(0.04, 0.58)	0.04	0	0.04	0
$\delta_{m2} = 0.2$	(0.04, 0.58)	0.04	-1	0.46	3
$k_{12} = 5 \times 10^{-5}$	$(1 \times 10^{-5}, 1.5 \times 10^{-4})$	$8.5 \times 10^{-5}$	-3	$1 \times 10^{-5}$	5
$k_{21} = 4 \times 10^{-5}$	$(8 \times 10^{-6}, 1.16 \times 10^{-5})$	$8 \times 10^{-6}$	-3	$5.6 \times 10^{-5}$	5
$a_{h1} = 8 \times 10^{-3}$	$(1.6 \times 10^{-3}, 2.32 \times 10^{-3})$	$1.6 \times 10^{-3}$	0	$1.6 \times 10^{-2}$	1
$a_{h2} = 8 \times 10^{-3}$	$(1.6 \times 10^{-3}, 2.32 \times 10^{-3})$	$1.6 \times 10^{-3}$	0	$1.6 \times 10^{-3}$	0
$r_{h1} = 9 \times 10^{-6}$	$(1.8 \times 10^{-7}, 2.61 \times 10^{-5})$	$1.8 \times 10^{-6}$	0	$9.9 \times 10^{-6}$	1
$r_{h2} = 9 \times 10^{-6}$	$(1.8 \times 10^{-7}, 2.61 \times 10^{-5})$	$1.8 \times 10^{-6}$	0	$1.8 \times 10^{-6}$	0
$\delta_{h1} = 0.05$	(0.01, 0.145)	0.01	0	0.01	0
$\delta_{h2} = 0.05$	(0.01, 0.145)	0.01	0	0.01	0
$\beta_{Th} = 1 \times 10^8$	$(2 \times 10^7, 2.9 \times 10^8)$	$2 \times 10^7$	0	$2 \times 10^7$	0

$$J = \begin{pmatrix} a_{11} & a_{12} & a_{13} & a_{14} & a_{15} & a_{16} \\ a_{21} & a_{22} & a_{23} & a_{24} & a_{25} & a_{26} \\ a_{31} & a_{32} & a_{33} & a_{34} & a_{35} & a_{36} \\ a_{41} & a_{42} & a_{43} & a_{44} & a_{45} & a_{46} \\ a_{51} & a_{52} & a_{53} & a_{54} & a_{55} & a_{56} \\ a_{61} & a_{62} & a_{63} & a_{64} & a_{65} & a_{66} \end{pmatrix},$$

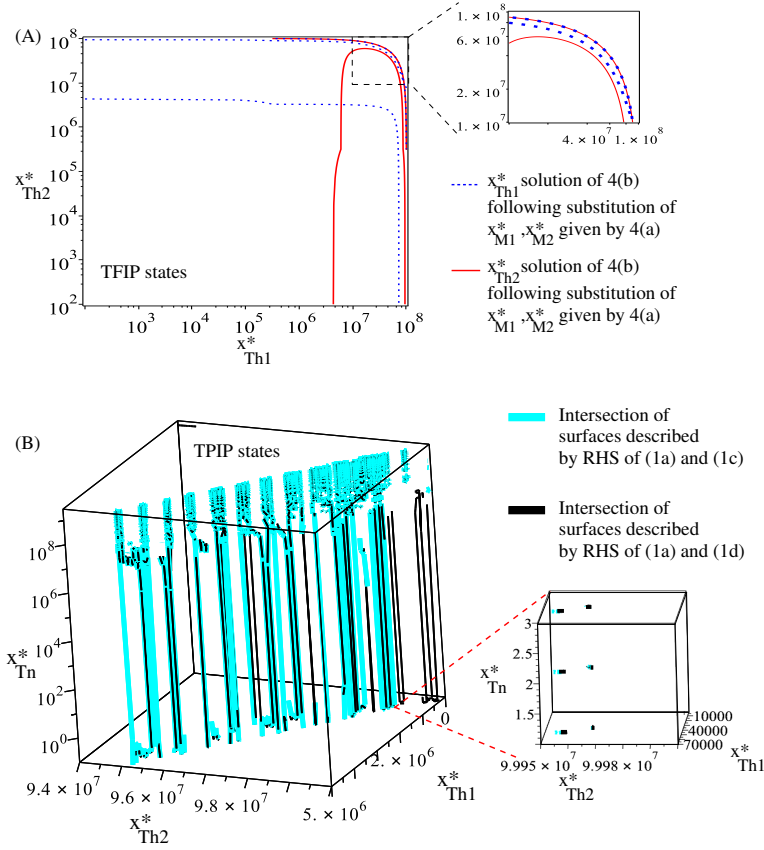


Figure B.13: Multiple TFIP and TPIP steady states. (A) The states  $x_{Th1}^*$  and  $x_{Th2}^*$  of the TFIP steady states (see eq. (4)), for  $k = k_{12}/k_{21} = 1.2$ . The inset shows a detailed picture of these states for  $x_{Th1}^*, x_{Th2}^* \in (10^7, 10^8)$ . The overlap of the continuous and dotted curves, for all  $x_{Th1}^*$  &  $x_{Th2}^*$  values within this interval, suggest the possibility of having an infinite number of steady states. (B) The TPIP states with  $x_{Ts}^* = 0$  is given by the intersection of the surfaces described by the right-hand-sides (RHS) of equations (1a)+(1c) (cyan curves; gray on black/white print) and RHS of equations (1a)+(1d) (black curves). Here, we consider  $k = k_{12}/k_{21} = 5$  (although different  $k$  generate similar curves). Note that there seems to be an infinite number of intersection points between the cyan and black curves. The inset shows the intersection points for  $x_{Tn}^* \in \{1, 2, 3\}$ .

590 with

$$\begin{aligned}
 a_{11} &= r \left( 1 - \frac{x_{Tn} + x_{Ts}}{\beta_T} \right) - r \frac{x_{Tn}}{\beta_T} - \delta_{mn} x_{M1} + r_{mn} x_{M2}, \quad a_{12} = -r \frac{x_{Tn}}{\beta_T} + k_{sn}, \\
 a_{13} &= -\delta_{mn} x_{Tn}, \quad a_{14} = r_{mn} x_{Tn}, \quad a_{15} = 0, \quad a_{16} = 0, \\
 a_{21} &= -r \frac{x_{Ts}}{\beta_T}, \quad a_{22} = r \left( 1 - \frac{x_{Tn} + x_{Ts}}{\beta_T} \right) - r \frac{x_{Ts}}{\beta_T} - k_{sn} - \delta_{ms} x_{M1} - \delta_{ts} x_{Th1}, \\
 a_{23} &= -\delta_{ms} x_{ts}, \quad a_{24} = 0, \quad a_{25} = -\delta_{ts} x_{Ts}, \quad a_{26} = 0, \\
 a_{31} &= 0, \quad a_{32} = a_s x_{M1} \left( 1 - \frac{x_{M1} + x_{M2}}{\beta_M} \right), \quad a_{36} = 0, \\
 a_{33} &= (a_{m1} x_{Th1} + a_s x_{Ts}) \left( 1 - \frac{2x_{M1} + x_{M2}}{\beta_M} \right) - \delta_{m1} - (k_{12} - k_{21}) x_{M2}, \\
 a_{34} &= -x_{M1} \left( \frac{a_{m1} x_{Th1} + a_s x_{Ts}}{\beta_M} + k_{12} - k_{21} \right), \quad a_{35} = a_{m1} x_{M1} \left( 1 - \frac{x_{M1} + x_{M2}}{\beta_M} \right),
 \end{aligned}$$

At the TF1IP steady state, in addition to the zero components already listed in equation (C.1), the following components of the Jacobian matrix are also zero:  $a_{13} = a_{14} = a_{21} = a_{23} = a_{25} = 0$ ,  $a_{41} = a_{43} = a_{46} = 0$ , and  $a_{65} = 0$ . For the baseline parameter values used throughout this article, eigenvalues  $\lambda_1 = a_{11} > 0$  and  $\lambda_2 = a_{22} > 0$  (since  $x_{M1}^* \approx 5805$  and  $x_{Th1}^* \approx 4333217$ ), and thus this state is always unstable. However, it could be possible that for different parameter values (e.g., much higher values of  $\delta_{mn}$ ,  $\delta_{ms}$ ,  $\delta_{ts}$ ),  $\lambda_{1,2} < 0$ . Then the stability could be influenced by the sign of  $\lambda_3 = a_{44} = x_{M1}(k_{12} - k_{21}) - \delta_{m2}$ :  $\lambda_3 > 0$  if  $k = k_{12}/k_{21} > 1$ , and  $\lambda_3 < 0$  otherwise.

At the TF2IP steady state, in addition to the zero components listed in equation (C.1), the following components of the Jacobian matrix are also zero:  $a_{13} = a_{14} = 0$ ,  $a_{21} = a_{23} = a_{25} = 0$ ,  $a_{32} = a_{34} = a_{35} = 0$ , and  $a_{56} = 0$ . Since eigenvalue  $\lambda_1 = x_{M2}^* r_{mn} + r > 0$ , the TF2IP state is always unstable.

The stability of the multiple TFIP steady states is difficult to investigate: e.g., one of the eigenvalues of the Jacobian matrix is  $\lambda_1 = a_{11} = -x_{M1}\delta_{mn} + x_{M2}r_{mn} + r$ . As shown in Figure B.13(a), some states have  $x_{M1} \gg x_{M2}$  and hence  $\lambda_1 < 0$ , while other states have  $x_{M1} \ll x_{M2}$  and hence  $\lambda_1 > 0$ .

The TO steady state is always unstable for the parameter values used in this article (since one eigenvalue is  $\lambda_1 = x_{Tn}a_n - \delta_{m2} > 0$ ).

For the TP1IP state, in addition to the zero components in equation (C.1), the following components of the Jacobian matrix are also zero:  $a_{21} = a_{23} = a_{25} = 0$ ,  $a_{41} = a_{43} = a_{46} = 0$ , and  $a_{65} = 0$ . The stability of this state is governed by the following eigenvalues:  $\lambda_1 = a_{11} < 0$ ,  $\lambda_2 = a_{22} < 0$ ,  $\lambda_3 = a_{44} = 90.213 + 5805.95(k_{12} - k_{21})$ ,  $\lambda_4 = a_{66} < 0$  and  $\lambda_{5,6} = 0.5(a_{33} + a_{55}) \pm 0.5\sqrt{(a_{33} + a_{55})^2 - 4(a_{33}a_{55} - a_{35}a_{53})}$ . For the baseline parameter values used throughout this article,  $k = k_{12}/k_{21} = 1.2 > 1$  which implies that  $\lambda_3 > 0$  and this state is unstable.

For the TP2IP state, in addition to the zero components in equation (C.1), the following components of the Jacobian matrix are also zero:  $a_{21} = a_{23} = a_{25} = 0$ ,  $a_{32} = a_{34} = a_{35} = 0$ , and  $a_{56} = 0$ . The stability of this state is governed by the sign of the following eigenvalues:  $\lambda_1 = a_{22} < 0$ ,  $\lambda_2 = a_{33} = -0.2 - 99808.35(k_{12} - k_{21})$ ,  $\lambda_3 = a_{55} < 0$  and  $\lambda_{4,5,6} < 0$  given by the three real roots of a cubic equation. If  $k = k_{12}/k_{21} > 1$  then  $\lambda_2 < 0$  and the TP2IP state is stable (as is the case for the baseline model). On the other hand, if  $k < 1$  then  $\lambda_2 > 0$  and the TP2IP state is unstable.

The stability of the TPIP states is difficult to investigate since, as shown in Figure B.13(b), there are multiple tumour states  $x_{Tn}^*$ . However, the stability of these states also depends on the ratio  $k = k_{12}/k_{21}$ .

## 629 References

- 630 Baba, T., Iwasaki, S., Maruoka, T., Suzuki, A., Tomaru, U., Ikeda, H.,  
631 Yoshiki, T., Kasahara, M., Ishizu, A., 2008. Rat CD4+CD8+ macrophages  
632 kill tumor cells through an NKG2D- and granzyme/perforin-dependent  
633 mechanism. *J Immunol* 180 (5), 2999–3006.
- 634 Bingle, L., Brown, N. J., Lewis, C. E., 2002. The role of tumour-associated  
635 macrophages in tumour progression: implications for new anticancer ther-  
636 apies. *J Pathol* 196 (3), 254–65.
- 637 Biswas, S. K., Mantovani, A., 2010. Macrophage plasticity and interaction  
638 with lymphocyte subsets: cancer as a paradigm. *Nat Immunol* 11 (10),  
639 889–896.
- 640 Carmona-Fontaine, C., Bucci, V., Akkari, L., Deforet, M., Joyce, J., Xavier,  
641 J., 2013. Emergence of spatial structure in the tumor microenvironment due  
642 to the Warburg effect. *Proc. Natl. Acad. Sci USA* 110 (48), 19402–19407.
- 643 Chen, P., Huang, Y., Bong, R., Ding, Y., Song, N., Wang, X., Song, X.,  
644 Luo, Y., 2011. Tumor-associated macrophages promote angiogenesis and  
645 melanoma growth via adrenomedullin in a paracrine and autocrine manner.  
646 *Clin Cancer Res* 17 (23), 7230–9.
- 647 Cillo, C., Dick, J., Ling, V., Hill, R., 1987. Generation of drug-resistant  
648 variants in metastatic B16 mouse melanoma cell lines. *Can. Res.* 47, 2604–  
649 2608.
- 650 Clear, A. J., Lee, A. M., Calaminici, M., Ramsay, A. G., Morris, K. J., Hal-  
651 lam, S., Kelly, G., Macdougall, F., Lister, T. A., Gribben, J. G., Jun. 2010.  
652 Increased angiogenic sprouting in poor prognosis FL is associated with el-  
653 evated numbers of CD163+ macrophages within the immediate sprouting  
654 microenvironment. *Blood* 115 (24), 5053–5056.
- 655 Diefenbach, A., Jensen, E. R., Jamieson, A. M., Raulet, D. H., 2001. Rae1  
656 and H60 ligands of the NKG2D receptor stimulate tumour immunity.  
657 *Nature* 413 (6852), 165–71.
- 658 Dunn, G., Old, L., R.D., S., 2004. The three Es of cancer immunoediting.  
659 *Annu. Rev. Immunol.* 22, 329–360.

660 Eftimie, R., Bramson, J., Earn, D., 2010. Modeling anti-tumor Th1 and Th2  
661 immunity in the rejection of melanoma. *J Theor Biol* 265 (3), 467–480.

662 Eikenberry, S., Thalhauser, C., Kuang, Y., 2009. Tumor-immune interac-  
663 tion, surgical treatment, and cancer recurrence in a mathematical model  
664 of melanoma. *PLoS Comput Biol* 5 (4), e1000362.

665 Ginhoux, F., Jung, S., 2014. Monocytes and macrophages: developmental  
666 pathways and tissue homeostasis. *Nat Rev Immunol* 14 (6), 392–404.

667 Gordon, S., Martinez, F., 2010. Alternative activation of macrophages: mech-  
668 anism and functions. *Immunity* 32, 593–604.

669 Gross, F., Metzner, G., Behn, U., 2011. Mathematical modelling of allergy  
670 and specific immunotherapy: Th1-Th2-Treg interactions. *J. Theor. Biol*  
671 269 (1), 70–78.

672 Hammes, L. S., Tekmal, R. R., Naud, P., Edelweiss, M. I., Kirma, N.,  
673 Valente, P. T., Syrjanen, K. J., Cunha-Filho, J. S., 2007. Macrophages, in-  
674 flammation and risk of cervical intraepithelial neoplasia (CIN) progression–  
675 clinicopathological correlation. *Gynecol Oncol* 105 (1), 157–65.

676 Herwig, M. C., Bergstrom, C., Wells, J. R., Holler, T., Grossniklaus, H. E.,  
677 2013. M2/m1 ratio of tumor associated macrophages and ppar-gamma  
678 expression in uveal melanomas with class 1 and class 2 molecular profiles.  
679 *Exp Eye Res* 107, 52–8.

680 Heusinkveld, M., van der Burg, S. H., 2011. Identification and manipulation  
681 of tumor associated macrophages in human cancers. *J Transl Med* 9, 216.

682 Hill, R., Chambers, A., Ling, V., Harris, J., 1984. Dynamic heterogeneity:  
683 rapid generation of metastatic variants in mouse B16 melanoma cells. *Sci-*  
684 *ence* 224 (4652), 998–1001.

685 Hung, K., Hayashi, R., Lafond-Walker, A., Lowenstein, C., Pardoll, D.,  
686 Levitsky, H., 1998. The central role of CD4(+) T cells in the antitumor  
687 immune response. *J Exp Med* 188 (12), 2357–68.

688 Kim, Y., Lee, S., Kim, Y., Lawler, S., Gho, Y., Kim, Y., Hwang, H.,  
689 2013. Regulation of Th1/Th2 cells in asthma development: a mathem-  
690 atical model. *Math. Biosci. Eng.* 10 (4), 1095–1133.

691 Kisseleva, E., Becker, M., Lemm, M., Fichtner, I., 2001. Early macro-  
692 phage and cytokine response during the growth of immunogenic and non-  
693 immunogenic murine tumours. *Anticancer Res.* 21 (5), 3477–3484.

694 Kogan, Y., Agur, Z., Elishmereni, M., 2013. A mathematical model for the  
695 immunotherapeutic control of the Th1/Th2 imbalance in melanoma. *Dis-  
696 crete and Continuous Dynamical Systems* 18 (4), 1017–1030.

697 Kuroda, M., 2010. Macrophages: do they impact AIDS progression more  
698 than CD4 T cells? *J. Leukoc. Biol.* 87, 569–573.

699 Laird, A., 1964. Dynamics of tumor growth. *Br. J. Cancer* 18, 490–502.

700 Leek, R. D., Lewis, C. E., Whitehouse, R., Greenall, M., Clarke, J., Harris,  
701 A. L., Oct. 1996. Association of macrophage infiltration with angiogenesis  
702 and prognosis in invasive breast carcinoma. *Cancer Research* 56 (20), 4625–  
703 4629.

704 Louzoun, Y., Xue, C., Lesinski, G., Friedman, A., 2014. A mathematical  
705 model for pancreatic cancer growth and treatments. *J. Theor. Biol.* 351,  
706 74–82.

707 Ma, J., Liu, L., Che, G., Yu, N., Dai, F., You, Z., 2010. The M1 form of  
708 tumor-associated macrophages in non-small cell lung cancer is positively  
709 associated with survival time. *BMC Cancer* 10, 112–120.

710 Mantovani, A., Romero, P., Palucka, A., F.M., M., 2008. Tumour immunity:  
711 effector response to tumour and role of the microenvironment. *Lancet* 371,  
712 771–783.

713 Mantovani, A., Sica, A., Sozzani, S., Allavena, P., Vecchi, A., Locati, M.,  
714 2004. The chemokine system in diverse forms of macrophage activation  
715 and polarisation. *TRENDS Immunol.* 25 (12), 771–783.

716 Mareel, M., Baetselier, P. D., Roy, F. V., 1991. Mechanisms of invasion and  
717 metastasis. CRC Press.

718 Mattes, J., Hulett, M., Xie, W., Hogan, S., Rothenberg, M., Foster, P.,  
719 Parish, C., 2003. Immunotherapy of cytotoxic T cell-resistant tumours by  
720 T helper 2 cells: An eotaxin and STAT6-dependent process. *J. Exp. Med*  
721 197 (3), 387–393.

722 McCarthy, E., 2006. The toxins of William B. Coley and the treatment of  
723 bone and soft-tissue sarcomas. *Iowa O* 26, 154–8.

724 Mills, C. D., 2012. M1 and M2 macrophages: Oracles of health and disease.  
725 *Crit Rev Immunol* 32 (6), 463–88, mills, Charles D eng *Crit Rev Immunol*.  
726 2012;32(6):463-88.

727 Nishimura, T., Iwakabe, K., Sekimoto, M., Ohmi, Y., Yahata, T., Nakui,  
728 M., T., S., Habu, S., H., T., Sato, M., Ohta, A., 1999. Distinct role of  
729 antigen-specific T helper type 1 (Th1) and Th2 cells in tumor eradication  
730 in vivo. *JEM* 190 (5), 617.

731 Noy, R., Pollard, J. W., 2014. Tumor-associated macrophages: From mech-  
732 anisms to therapy. *Immunity* 41 (1), 49–61.

733 Ohri, C. M., Shikotra, A., Green, R. H., Waller, D. A., Bradding, P., 2009.  
734 Macrophages within NSCLC tumour islets are predominantly of a cyto-  
735 toxic M1 phenotype associated with extended survival. *Eur Respir J* 33 (1),  
736 118–126.

737 Pepper, M., Jenkins, M. K., 2011. Origins of CD4(+) effector and central  
738 memory T cells. *Nat Immunol* 12 (6), 467–71.

739 Perez-Diez, A., Joncker, N., Choi, K., Chan, W., Anderson, C., Lantz, O.,  
740 Matzinger, P., 2007. CD4 cells can be more efficient at tumor rejection  
741 than CD8 cells. *Blood* 109, 5346–5354.

742 Ribeiro, R. M., Mohri, H., Ho, D. D., Perelson, A. S., 2002. In vivo dynamics  
743 of T cell activation, proliferation, and death in HIV-1 infection: why are  
744 CD4+ but not CD8+ T cells depleted? *Proc Natl Acad Sci USA* 99 (24),  
745 15572–7.

746 Romagnani, S., 1999. Th1/Th2 cells. *Inflamm. Bowel Dis.* 5 (4), 285–294.

747 Rosenberg, S., Yang, J., Restifo, N., 2004. Cancer immunotherapy: moving  
748 beyond current vaccines. *Nature Medicine* 10 (9), 909–915.

749 Schreiber, R. D., Old, L. J., Smyth, M. J., 2011. Cancer immunoediting:  
750 integrating immunity’s roles in cancer suppression and promotion. *Science*  
751 331 (6024), 1565–70.



- 752 Sica, A., Bronte, V., 2007. Altered macrophage differentiation and immune  
753 dysfunction in tumor development. *J. Clin. Investigation* 117 (5), 1155–  
754 1166.
- 755 Sica, A., Mantovani, A., 2012. Macrophage plasticity and polarization: in  
756 vivo veritas. *J Clin Invest* 122 (3), 787–95.
- 757 Steidl, C., Lee, T., Shah, S. P., Farinha, P., Han, G., Nayar, T., Delaney,  
758 A., Jones, S. J., Iqbal, J., Weisenburger, D. D., Bast, M. A., Rosenwald,  
759 A., Muller-Hermelink, H.-K., Rimsza, L. M., Campo, E., Delabie, J., Bra-  
760 ziel, R. M., Cook, J. R., Tubbs, R. R., Jaffe, E. S., Lenz, G., Connors,  
761 J. M., Staudt, L. M., Chan, W. C., Gascoyne, R. D., Mar. 2010. Tumor-  
762 associated macrophages and survival in classic Hodgkin’s lymphoma. *The*  
763 *New England Journal of Medicine* 362 (10), 875–885.
- 764 Tang, X., Mo, C., Wang, Y., Wei, D., Xiao, H., 2013. Anti-tumour strategies  
765 aiming to target tumour-associated macrophages. *Immunology* 138 (2),  
766 93–104.
- 767 Van Furth, R., 1989. Origin and turnover of monocytes and macrophages.  
768 *Curr. Top. Pathol.* 79, 125–150.
- 769 Wang, Y., Yang, T., Ma, Y., Halade, G., Zhang, J., Lindsey, M., Jin, Y.-  
770 F., 2012. Mathematical modelling and stability analysis of macrophage  
771 activation in left ventricular remodelling post-myocardial infarction. *BMC*  
772 *Genomics* 13 (Suppl. 6).
- 773 Welsh, T., Green, R., Richardson, D., Waller, D., O’Byrne, K., Bradding,  
774 P., 2005. Macrophage and mast-cell invasion of timor cell islets confers a  
775 marked survival advantage in non-small-cell lung cancer. *J. Clin. Oncol.*  
776 23 (35), 8959–8967.
- 777 Xu, W., Liu, L., Loizidou, M., Ahmed, M., Charles, I., 2002. The role of  
778 nitric oxide in cancer. *Cell Res.* 12 (5-6), 311–320.
- 779 Zeni, E., Mazzetti, L., Miotto, D., Lo, C., Maestrelli, P., Querzoli, P., Pedri-  
780 ali, M., De Rosa, E., Fabbri, L., Mapp, C., Boschetto, P., 2007. Macro-  
781 phage expression of interleukin-10 is a prognostic factor in nonsmall cell  
782 lung cancer. *Eur. Respir.* 30, 627–632.

- 783 Zhang, M., He, Y., Sun, X., Li, Q., Wang, W., Zhao, A., Di, W., 2014.  
784 A high M1/M2 ratio of tumor-associated macrophages is associated with  
785 extended survival in ovarian cancer patients. *J Ovarian Res* 7, 19.
- 786 Zijlmans, H. J. M. a. A., Fleuren, G. J., Baelde, H. J., Eilers, P. H. C., Kenter,  
787 G. G., Gorter, A., Mar. 2006. The absence of CCL2 expression in cervical  
788 carcinoma is associated with increased survival and loss of heterozygosity  
789 at 17q11.2. *The Journal of Pathology* 208 (4), 507–517.